bioRχiv

Convergent gene expression in epithelial cells illuminates the evolution of uterine receptivity

Axelle Brulport[1,*,#], Małgorzata Anna Gazda[1,a,*], Maëlle Daunesse[1,2,†], Eulalie Liorzou[1,†], Bruno Raquillet[1], Anthony Lepelletier[1], Maria Sopena-Rios[1,b], Mariam Raliou[3], Pierrick Regnard[4], Lyne Fellmann[4], Lucie Faccin[5], Slaveia Garbit[5], Alexia Cermolacce[5], Ivanela Kondova[6], Louis Marcellin[7,8,9], Carole Abo[7,8,9], Ludivine Doridot[10], Camille Berthelot[1,#]

[1]Institut Pasteur, Université Paris Cité, CNRS UMR 3525, INSERM UA12, Comparative Functional Genomics group, F-75015 Paris, France.
[2]European Molecular Biology Laboratory, European Bioinformatics Institute, Wellcome Trust Genome Campus, Hinxton, Cambridge, CB10 1SD, UK.
[3]Université Paris-Saclay, UVSQ, INRAE, BREED, 78350, Jouy-en-Josas, France.
[4]SILABE – Université de Strasbourg, Fort Foch, 67207 Niederhausbergen, France
[5]Station de Primatologie - CNRS - UAR 846, 2230 route des Quatre Tours, 13790 Rousset sur Arc, France.
[6]Biomedical Primate Research Centre (BPRC), Animal Science Department, Division of Pathology and Microbiology, Rijswijk, The Netherlands
[7]Université de Paris Cité, Faculté de Médecine, Paris, France.
[8]Department of Gynecology Obstetrics II and Reproductive Medicine (Professor Chapron), Assistance Publique-Hôpitaux de Paris (AP-HP), Hôpital Universitaire Paris Centre (HUPC), Centre Hospitalier Universitaire (CHU) Cochin, Paris, France.
[9]Department "Development, Reproduction and Cancer", Cochin Institute, INSERM U1016, Paris, France.
[10]Université Paris Cité, Institut Cochin, INSERM, CNRS, F-75014 PARIS, France, Paris, France.
[a]Current address: Department of Biological Sciences, University of Montréal, 1375 Avenue Thérèse-Lavoie-Roux, H3C 3J7 Montréal, Québec, Canada.
[b]Current address: Life Sciences Department, Barcelona Supercomputing Center, 08034, Barcelona, Catalonia, Spain.
*Joint first authors
†Joint second authors
#Correspondence should be addressed to A.B and C.B. (axelle.brulport@inserm.fr and camille.berthelot@pasteur.fr)

The independent evolution of convergent embryo implantation mechanisms in humans and mice, differing from the ancestral mammalian phenotype, is poorly understood. Endometrial epithelial cells are the first maternal interface encountered by the embryo. We combined organoid models and single-cell transcriptomics to investigate how gene expression has evolved in endometrial epithelial cells between human, non-human primates, and mouse at key points in the hormonal cycle. We discovered that many maternal genes involved in uterine receptivity and embryo implantation exhibit more similar expression patterns between human and mouse compared to macaque and marmoset. In particular, we show that the endometrial expression of *LIF*, a crucial actor of endometrial receptivity in both human and mouse, is likely an evolutionary convergence rather than a conserved feature as previously hypothesised.

Introduction

The uterus is a key organ of the mammalian female reproductive tract, with crucial roles in embryo implantation, placenta development, pregnancy support and parturition. The uterus is composed of two tissue layers: the myometrium, a thick-walled smooth muscle with supportive and contractile functions; and the endometrium, a dynamic mucosa that experiences rapid tissue growth and differentiates to become receptive to embryo implantation (Critchley et al. 2020). This cyclical remodelling of the endometrium is orchestrated by ovarian steroid hormones (oestrogen and progesterone), which are themselves regulated by the hypothalamus-pituitary axis (Critchley et al. 2020). Despite its paramount importance for successful reproduction and species survival, the evolution of the mammalian uterus remains poorly understood. The tissular structures and cellular composition of the uterus are conserved across mammals, as is the overall sequence of the hormonal cycle; however, mammalian evolution is also marked by important differences in uterine morphology and physiology between species (Machado, Ontiveros, and Behringer 2022). These shifts include different mechanisms of embryo attachment and implantation into the receptive maternal endometrium (Muter et al. 2023; Siriwardena and Boroviak 2022; McGowen et al. 2014), as well as dramatic differences in placental invasivity into the uterine wall and in placental structures (Roberts, Green, and Schulz 2016; Carter and Enders 2004). Capturing and comparing the molecular tenets of these time- and hormone-dependent processes in vivo across multiple species remains a major challenge.

Of the two main cell types that compose the endometrium, only the evolution of stromal cells has been investigated at the molecular level. Endometrial stromal cells are fibroblasts that differentiate into decidual cells following hormonal and

embryonic cues to participate in placenta establishment (Critchley et al. 2020). Transcriptomic comparisons of endometrial stromal cell lines across species have illuminated the functional bases of key mammalian adaptations such as decidualization (Lynch et al. 2011; Erkenbrack et al. 2018; Mika et al. 2022). How endometrial epithelial cells have evolved remains however largely unexplored (Muter et al. 2023). The endometrial epithelium, a continuous epithelial cell layer lining the uterine lumen and glands, plays fundamental roles in embryo recognition and early implantation (Muter et al. 2023), stromal decidualization (Filant and Spencer 2013), and immunity against pathogens in the uterine cavity (King, Critchley, and Kelly 2003). As such, endometrial epithelial cells are thought to be a key player in the evolutionary changes in uterine receptivity and embryo implantation strategies observed in mammals.

Endometrial epithelial organoids are an emerging model to study the functions of primary endometrial epithelial cells. Grown from tissue-derived stem cells seeded into an artificial extracellular matrix, these 3D epithelial structures recapitulate many of their in vivo characteristics, differentiating into secretory and ciliated cellular subtypes and secreting uterine fluid-like mucus (M. Y. Turco et al. 2017; Boretto et al. 2017). Here, we examine the evolution of gene expression in endometrial epithelial cells by leveraging endometrial epithelial organoids as well as single-cell transcriptomics on timed endometrial biopsies across three model mammals: human, mouse, and macaque, a non-human primate and model species for female reproductive biology. Humans and macaques share many characteristics in their reproductive cycles and strategies, while mice differ significantly. However, human and mouse have convergently evolved interstitial mechanisms of embryo implantation, where the blastocyst interacts with maternal cells to become fully embedded into the endometrium (Muter et al. 2023; Siriwardena and Boroviak 2022; McGowen et al. 2014). Macaque, like most primates except great apes, undergoes superficial implantation, where the embryo remains inside the uterine cavity and only superficially breaches into maternal tissues (Siriwardena and Boroviak 2022). How maternal endometrial epithelial cells prepare for embryo implantation in different species is not understood: here, we investigate whether this first line of cellular contact between maternal and embryonic tissues has evolved convergent molecular traits between human and mouse that may underlie the similarity of their implantation phenotypes.

Results

Endometrial epithelial organoids from a non-human primate recapitulate uterine epithelium phenotypes

To investigate the evolution of the endometrial epithelium, we derived endometrial epithelial organoids from fresh endometrial biopsies of three cynomolgus macaques (Macaca fascicularis) and three genetically diverse mice strains (Mus musculus), following previously published protocols for human and mouse (Fig. 1A; Methods) (Boretto et al. 2017; 2019; Margherita Y. Turco et al. 2017). After two days of culture, we obtained endometrial epithelial organoids for both species, which continued to grow and increase in size over time, and exhibited the characteristic structure previously reported in human (Boretto et al. 2019; Margherita Y. Turco et al. 2017) and mouse (Boretto et al. 2017) endometrial epithelial organoids. Macaque organoids displayed the same cellular organisation as human and mouse organoids, with a polarised peripheral epithelial layer (E-Cadherin positive) surrounding a central lumen, and were proliferative (Ki-67 positive; Fig. 1B). These represent to our knowledge the first lines of non-human primate endometrial epithelial organoids, modelling the luminal epithelium and glands found in the macaque uterine endometrium.

We next investigated how macaque organoids respond to oestrogen and progesterone, by mimicking the hormonal exposure that uterine cells experience in vivo. The hormonal cycle is largely conserved between mammals (Critchley et al. 2020; McLean et al. 2012; Silvestri and Fraser 2007; Kromrey, Czoty, and Nader 2015; Huchard et al. 2009), with a first proliferative phase driven by oestrogen (E2) and a second secretory phase where endometrial cells experience differentiation under the effects of progesterone (P4) (Critchley et al. 2020). After five days of growth, we exposed macaque and mouse organoids to E2 for 48 hours, or to E2 for 48 hours followed by P4 for another 48 hours (Boretto et al. 2017) (Fig. 1A). Hormonal treatment modifies the phenotype of macaque and mouse endometrial organoids, which acquire a brown, dark colour, with modification of their 3D conformation and reduced growth (Fig. 1C). Hormone-treated organoids grew significantly more slowly than untreated controls in both species (Fig. 1D; linear model: macaque: $p = 0.01$; mouse: $p = 0.01$).

We then explored whether macaque endometrial organoids express known functional markers of hormonal response. As observed in human (Boretto et al. 2017; 2019; Margherita Y. Turco et al. 2017) and mouse (Boretto et al. 2017), macaque organoids secrete mucus upon stimulation by oestrogen and progesterone, as evidenced by Periodic Acid Schiff (PAS) staining (Fig. 1E). Macaque organoids also express the oestrogen receptor (ESR1) after both E2 and P4 treatment, and the progesterone receptor (PGR) after E2 treatment only (Fig. 1E), consistent with previous histological analysis on human tissue which showed that PGR is down-regulated in the mid and late luteal phase with no expression in the functional glands (Mehasseb et al. 2011). We also observed the presence of ciliated epithelial cells after E2 and P4 treatment, as evidenced by acetyl-α tubulin labelling, suggesting the presence of diverse epithelial cell types as observed in vivo in endometrial tissue (Fig. 1E). Our phenotypic observations confirm that macaque endometrial epithelial organoid lines are functional and faithfully reproduce previously described in vivo characteristics in response to hormonal treatment in human (Boretto et al. 2017; 2019; Margherita Y. Turco et al. 2017) and mouse (Boretto et al. 2017).

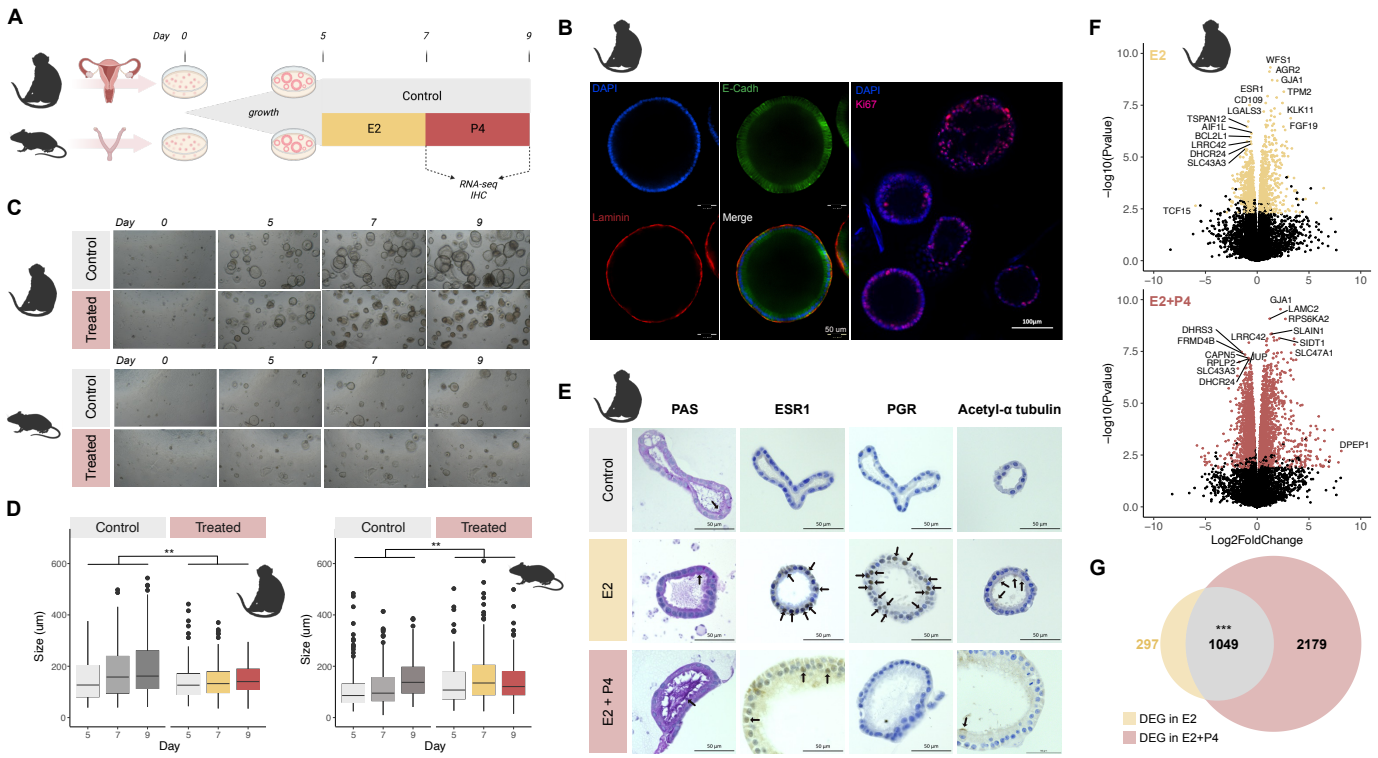

Figure 1: Establishment of hormone-responsive epithelial organoids from macaque uterine endometrium. (A) Experimental design and hormonal stimulation timeline. Endometrial epithelial organoids were grown from macaque and mouse endometrial tissue samples in growth medium from day 0 to day 5, primed with E2 for 48h, then stimulated with P4 for 48h (termed E2+P4 thereafter). **(B)** Immunofluorescence staining of untreated macaque endometrial epithelial organoids for E-cadherin (epithelial cell marker), laminin (basement membrane marker) and Ki-67 (proliferation marker), x40. **(C)** Growth of control and treated endometrial epithelial organoids monitored over time for both species after seeding (day 0), after growth step (day 5), after E2 treatment (day 7) and after P4 treatment (day 9), x10. **(D)** Diameters of macaque and mouse organoids before treatment (day 5), after E2 treatment (day 7) and after E2+P4 treatment (day 9). **: p-values < 0.01, ANOVA. **(E)** Periodic Acid Schiff staining of mucin (arrows), and immunohistochemistry staining for steroid hormone receptors (ESR1 and PGR; arrows) and acetylated a-tubulin to visualise cilia (arrows), x40. **(F)** Differentially expressed genes (DEGs) in response to E2 (yellow) or E2+P4 (red) treatment in macaque organoids, compared to untreated controls. Gene names are reported for the top 10 up- and down-regulated genes based on highest euclidean distance to 0. **(G)** Overlap of macaque DEGs after E2 and E2+P4 treatments. *** = p-value < 0.001, hypergeometric test.

To understand how endometrial organoids respond to hormones in mammalian models for reproductive biology, we sequenced the transcriptomes of hormone-treated and control organoids from macaque and mouse (Fig. 1A) for comparison with two publicly available RNA-seq datasets from human endometrial epithelial organoids in similar hormone stimulation experiments (Methods). Principal component analysis (PCA) revealed that transcriptomic profiles clearly distinguish between control and hormone-treated organoids in all three species (Fig. S1). We identified 630, 1,346 and 2,520 differentially expressed genes (DEGs) after E2 treatment and 4,472, 3,228 and 2,322 after E2+P4 treatment in human, macaque and mouse, respectively. (Fig. 1F, S2; Methods). Examining the function of the top DEGs across species revealed key actors of endometrial receptivity (PGR, ESR1, Asgr2, RPLP2) (Wetendorf et al. 2017; Cha, Sun, and Dey 2012; Forde et al. 2011; Manohar et al. 2014), embryo implantation (KLK11, TPPP3, CDC20B, Gper1) (Wetendorf et al. 2017; Cha, Sun, and Dey 2012; Fernando et al. 2006; Kolkova et al. 2010; Yan and Clarke 2017), decidualization (TPPP3, Gper1, GJA1, PLXNA4, C1rb, Ceacam10) (Kaya et al. 2015; Garrido-Gomez et al. 2021; Shukla et al. 2019; Kolkova et al. 2010; Yu et al. 2017; Manley et al. 2020; Xu et al. 2022; Sones et al. 2018; Finkenzeller et al. 2003), pregnancy outcomes (GSTA3, Kcnj1) (Garrido-Gomez et al. 2021; 2017; Lundgren et al. 1997) and endometrial dynamic changes during the menstrual cycle (ESR1, PGR, DEUP1, LGALS3) (Gleeson et al. 1993; Spassky and Meunier 2017; Okumu et al. 2011). Additionally, in each species, around 75% of genes differentially expressed under E2 treatment were also DEGs after E2+P4 treatment (Fig. 1G, S3), suggesting that we capture a continuous response of endometrial epithelial organoids to E2 and E2+P4 hormonal exposure. The successful establishment of functional macaque endometrial epithelial organoids reported here therefore presents an opportunity to investigate the evolutionary dynamics of the uterine epithelium transcriptome in mammals.

The evolution of transcriptomic responses to hormones reveals conserved functional pathways in the endometrial epithelium between mammals

To compare gene expression between human, macaque and mouse, we identified 15,015 one-to-one orthologous genes across the three species (Methods). Transcriptome comparison supports that the identity of endometrial epithelial cells is largely conserved between primates and mice, with a generally high correlation of their gene expression levels (Spearman correlation; human-macaque: $\rho = 0.75$; human-mouse: $\rho = 0.71$; macaque-mouse: $\rho = 0.80$; Fig. 2A) and as previously observed in other tissues and cell types (Murat et al. 2023; Sepp et al. 2024). PCA revealed that the two first

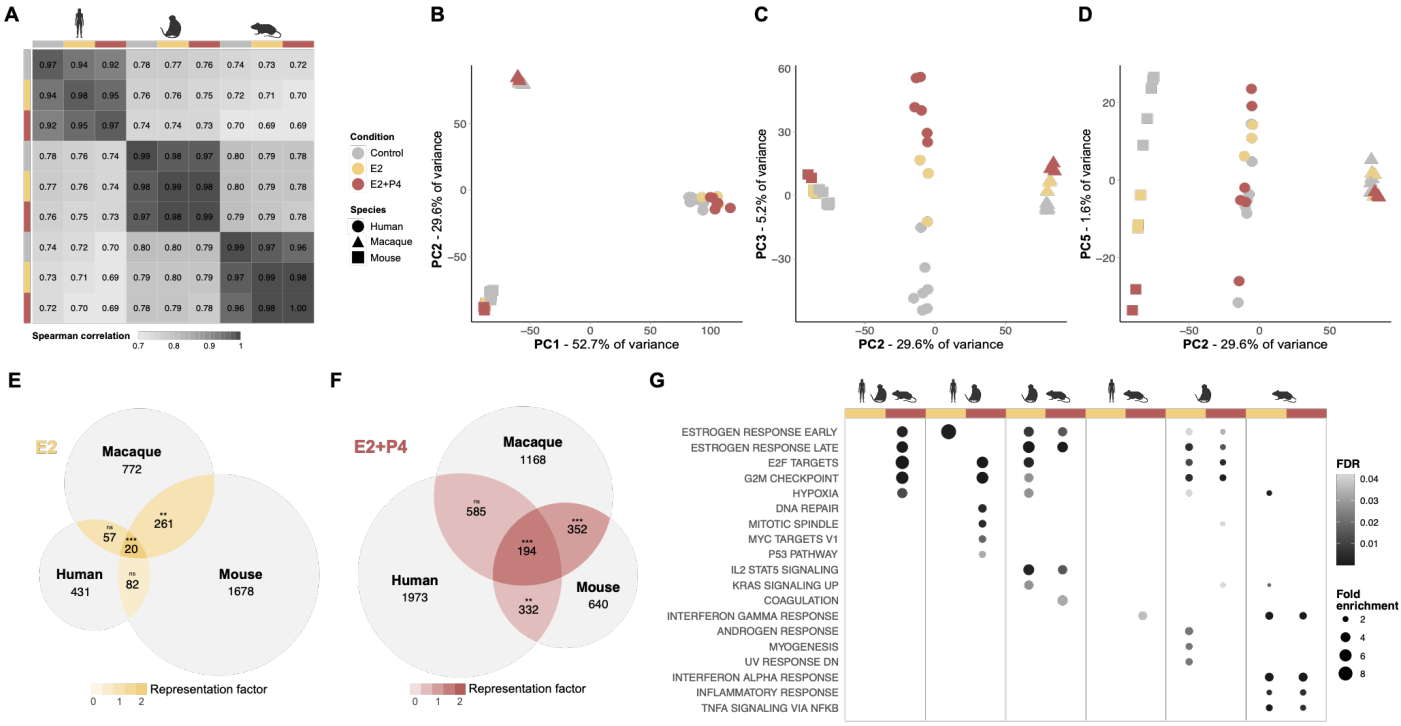

Figure 2: Endometrial epithelial cell transcriptomes are overall conserved between model mammals but display divergences in hormonal response. (A) Gene expression correlations across conditions and species. Each coefficient represents the mean Spearman rho coefficient across all pairwise correlations of biological replicates per condition and species. **(B-C-D)** Principal component analysis of gene expression across 15,015 one-to-one orthologues between all three species. **(B)** Principal components 1 and 2, (C) PC 2 and 3, **(D)** PC 2 and 4. **(E-F)** Differentially expressed genes shared between human, macaque and mouse **(E)** after E2 treatment, **(F)** after E2+P4 treatment. Colour intensity represents the representation factor, e.g. observed to expected overlap. *: p-values < 0.05, **: p-values < 0.01 and ***: p-values < 0.001, hypergeometric test, BH adjustment. (G) Hallmark gene sets annotations over-represented in genes differentially expressed in all species, in any pair of species, or only in one species in response to hormonal treatment. P-values were calculated using a hypergeometric test followed by false discovery rate (FDR) correction.

principal components (PC) separate the transcriptomes by species, and together explained 82.3% of the total variance in gene expression (Fig. 2B). Gene expression changes induced by hormonal treatment in each species were minor compared to the divergence in gene expression accumulated over evolutionary time. PC3 correlates with treatments in human and macaque samples and explains 5.2% of the total gene expression variance (Fig. 2C). Mouse samples did not separate strongly along PC3, but aligned with treatment along PC5 (1.6% of total variance; Fig. 2D). These results suggest that primate endometrial epithelial cells share common features in their response to E2 and P4, which are not conserved in mouse cells.

We then investigated whether hormonal treatment induces changes in gene expression shared across the three species. We identified a core set of differentially expressed genes common to all species after each treatment (E2: 20 genes; E2+P4: 194 genes; Fig. 2E-F, Table S1), as well as subsets of DEGs shared by any pair of species. Functional enrichment analysis using Hallmark gene sets (Liberzon et al. 2015) revealed that genes responding to hormones and shared between species are enriched in pathways involved in cell growth (E2F target, G2M checkpoint, DNA repair, mitotic spindle, KRAS signalling) but also and more interestingly, in functions with key roles for maternal preparation to embryo implantation (Fig. 2G, Table S2; Methods). These include oestrogen response, hypoxia pathways (Martínez-Aguilar et al. 2021), the p53 pathway (Hu et al. 2007; Kang and Rosenwaks 2018), inflammation (interferon gamma response)(Q. Li et al. 2001; Murphy et al. 2009) and immune signalling pathways (IL2 STAT5 signalling) (Fainboim and Arruvito 2011; Lamprianidou et al. 2020). Amongst those shared DEGs, we identified several proposed biomarkers for endometrial receptivity such as GADD45A and MAOA (Altmäe et al. 2017). Species-specific DEGs were also enriched in inflammatory and immune response genes. Altogether, and in all three species, hormonal stimulation modifies a range of functional pathways with described roles in embryonic implantation, consistent with the role of endometrial epithelial cells as the first line of contact with the implanting blastocyst in mammals. Embryonic implantation however proceeds differently across our three study species. Human and mouse have convergently evolved an interstitial mode of embryo implantation, where the blastocyst breaches through the endometrial epithelium and becomes fully embedded into the maternal mucosa (Muter et al. 2023; Siriwardena and Boroviak 2022; McGowen et al. 2014). Macaque on the other hand displays superficial embryo implantation, where the blastocyst remains at the endometrium surface before placentation proceeds, which is the ancestral phenotype of primates (Siriwardena and Boroviak 2022; McGowen et al. 2014). In the next paragraphs, we take advantage of this experimental design to explore in more detail how ovarian hormones prime maternal epithelial cells for embryo implantation in species that have evolved different strategies of embryonic implantation.

Maternal embryo implantation genes are convergently activated in human and mouse endometrial epithelial organoids

Uterine receptivity and endometrial preparation to embryo implantation are poorly annotated in functional databases, which limits our ability to dissect how implantation preparation pathways have evolved in endometrial cells. To circumvent this, we curated a list of 59 genes with well-described roles in uterine receptivity, embryo attachment and embryo implantation in mammalian endometrial epithelial cells from the literature, termed "Implantation", which we added as an additional process to the analysis (Table S3; Methods).

To further explore whether cellular processes are similarly activated or repressed in response to hormonal stimulation across human, macaque and mouse, we extracted all genes annotated to the functions highlighted in Fig. 2G, regardless of whether they are detected as differentially expressed. We then tested whether expression fold-changes of these genes in response to hormonal stimulation were correlated across species. Human and macaque organoids displayed stronger correlations in gene expression fold-changes for most processes, consistent with their closer phylogenetic distance (Fig. 3A). Cell cycle processes showed high correlations between all conditions except in human organoids after E2 treatment, where they were anti-correlated to other samples. This may reflect a difference in cell expansion dynamics of human epithelial cells in response to oestrogen specifically, or could also reflect a technical effect, as these samples were processed externally to our lab. Pathways related to hormone response showed higher correlation within primates (Fig. 3A), in line with our previous observation that both human and macaque cells exhibit a common gene expression response overall to hormonal treatment (Fig. 2C). In contrast, genes involved in maternal preparation to implantation and the p53 pathway showed significant correlations in expression fold-changes between human and mouse, which were not shared with macaque (Fig. 3A). Interestingly, the p53 pathway has a documented role during implantation in both human (Kang and Rosenwaks 2018) and mouse (Hu et al. 2007), and influences the endometrial expression of the Leukemia Inhibitory Factor (*LIF*) (Hu et al. 2007), an interleukin family 6 cytokine pivotal to maternal-embryonic crosstalk and early implantation (Salleh and Giribabu 2014; Rosario and Stewart 2016).

Because genes involved in maternal preparation to implantation display an unusual pattern of expression convergence between human and mouse, we next sought to identify additional candidates by exhaustively searching for similar convergent expression patterns. We performed a Weighted Gene Correlation Network Analysis (WGCNA, Methods) which identified 8 modules of co-expressed genes, where the three largest modules reflect stronger expression similarities between either human and macaque, human and mouse, or macaque and mouse (Fig. 3B, S4). Module 1 corresponds to a group of 3,727 genes more similar in expression between

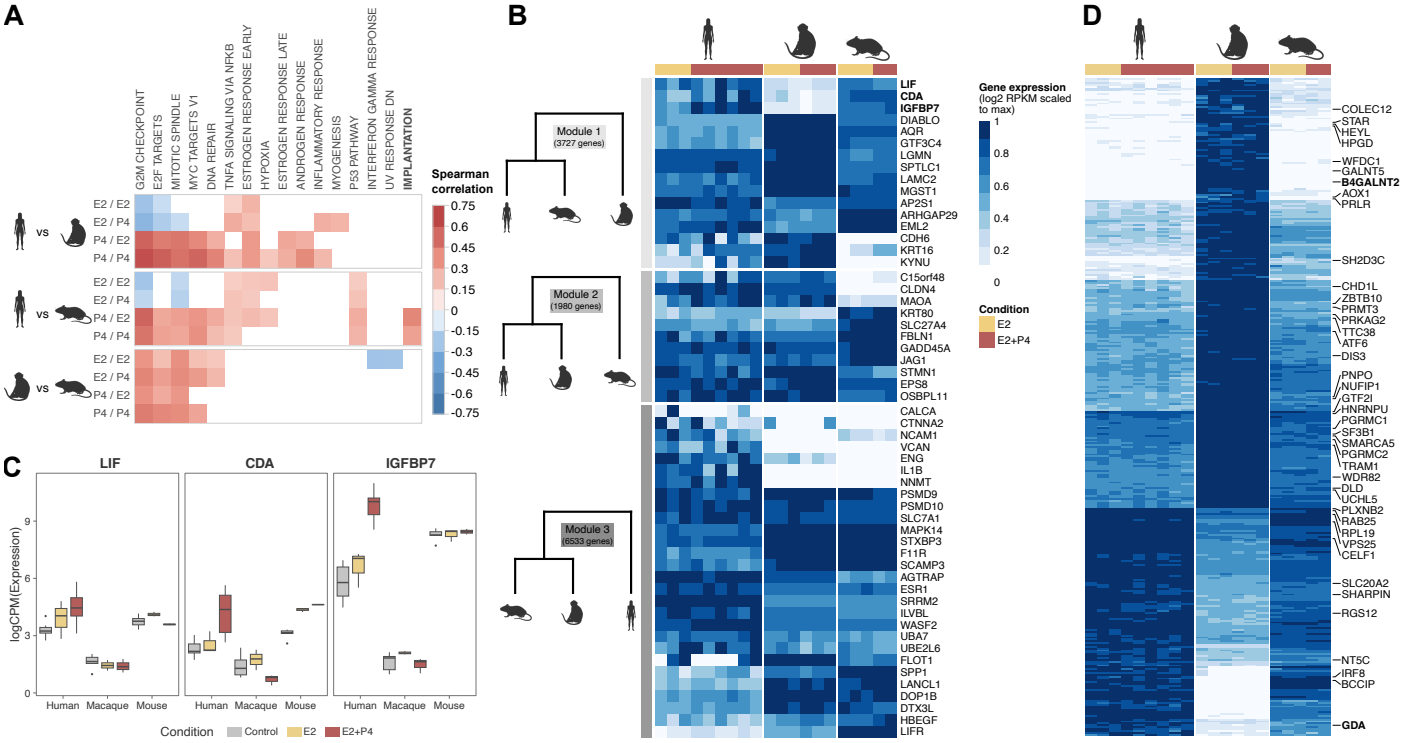

Figure 3: Maternally-expressed genes related to embryo implantation share similar expression patterns in human and mouse compared to macaque. (A) Pairwise correlations of expression log2-fold-changes in response to E2 or E2+P4 treatment compared to controls, for all genes annotated to over-represented Hallmark gene sets, as well as maternally-expressed genes with documented roles in endometrial receptivity and embryo implantation (termed 'Implantation'). Only correlations with a BH-adjusted p-value < 0.1 are represented. **(B)** Expression of maternal implantation genes across treatments in human, macaque and mouse endometrial epithelial organoids (normalised RPKM, log2-transformed, scaled to the maximum expression value for each gene). Genes are divided in three groups, corresponding to the main modules obtained in the co-expression analysis (Methods), which reflect differences in phylogenetic similarity as shown on the left. **(C)** Normalised expression levels for *LIF*, *CDA* and *IGFBP7* across treatments and species. **(D)** Normalised expression levels for 352 genes strongly co-expressed with *LIF* (co-expression weight > 0.4). Labelled genes have documented roles in endometrial receptivity, decidualization, embryo implantation, pregnancy outcomes and ovarian hormone response. Log2-transformed expression levels are scaled to the maximum value for each gene for representation.

human and mouse than with macaque. Sixteen genes involved in implantation are in Module 1, and in particular *LIF*, *CDA* and *IGFBP7*, which are expressed in human and mouse epithelial organoids but exhibit low expression in macaque (Fig. 3C). *LIF* is essential to successful pregnancy establishment, and is generally thought to be a deeply conserved actor of embryo implantation in mammals due to its importance for uterine receptivity in both human and mouse (Salleh and Giribabu 2014; Rosario and Stewart 2016). The low expression of *LIF* in macaque epithelial cells after hormonal stimulation was therefore striking, and suggests a potentially profound difference in maternally-controlled mechanisms of endometrial receptivity and preparation to embryo implantation. *CDA* and *IGFBP7* have been overall less described, but also have documented roles in endometrial receptivity (Evans et al. 2020; Díaz-Gimeno et al. 2011; Liu et al. 2012; Domínguez et al. 2003). To identify other candidate genes of potential interest within Module 1, we prioritised 352 genes most strongly co-expressed with *LIF* (weight > 0.4; Table S4). Many of these candidate genes have been previously described as involved in the processes of endometrial decidualization and implantation (*HEYL*, *VPS25*, *RGS12*, *GDA*, *SHARPIN*, *EIFAEBP1*, *RPL19*, *IRF8*, *HPGD*, *SF3B1*, *DIS3*, *GTF2I*, *SMARCA5*, *PGRMC1*, *COLEC12*, *PRLR*, *GALNT5*, *B4GALNT2*, *PRMT3*, *CELF1*, *SH2D3C*, *ATF6*, *UCHL5*, *GNA12*) and pregnancy outcomes (*PLXNB2*, *RAB25*, *TRAM1*, *SLC20A2*, *PRLR*, *CHD1L*, *WDR82*, *TTC38*, *DLD*, *PRKAG2*, *BCCIP*, *AGGFI*, *NUFIP1*), or are regulated by oestrogen and/or progesterone (*PNPO*, *NT5C*, *RAB25*, *HNRNPU*, *WFDC1*, *AOX1*, *STAR*, *ZBTB10*, *PGRMC2*) (Fig. 3C).

These analyses revealed that a large panel of known actors in endometrial receptivity and maternal preparation to embryo implantation, notably *LIF*, present more similar expression and hormone-triggered variations between human and mouse than between human and macaque. These differences in gene expression are therefore functional candidates that may have contributed to the convergent evolution of interstitial embryo implantation mechanisms in human and mouse, which both differ from macaque, where implantation is superficial.

Single-cell transcriptomics of the endometrium confirms a convergent evolution of epithelial gene programs in human and mouse

While our previous analyses highlight candidate genes that may have experienced convergent expression changes in human and mouse, other interpretations may also explain those results: first and foremost, endometrial organoids may not faithfully replicate gene expression in vivo. Second, gene expression at these loci may not be appropriately quantified because of annotation issues, in particular in the reference cynomolgus macaque genome. Finally, these differences in gene expression may be macaque-specific traits, unshared with other primates that also exhibit superficial implantation. To address those potential caveats, we performed single-nucleus transcriptome sequencing in endometrial samples from a rhesus macaque, a marmoset and a mouse, collected in unfecundated cycling female individuals during the late secretory phase of the uterine cycle, when the endometrium becomes receptive to embryo implantation (Methods). Additionally, we used the single-cell transcriptomes of human endometrial samples in the late secretory phase available from the Reproductive Cell Atlas (Garcia-Alonso et al. 2021). Marmoset is a platyrrhine (New World monkey) that also presents a superficial embryonic implantation phenotype, which is the likely ancestral phenotype in primates (Enders and Lopata 1999), while rhesus macaque is a sister species to cynomolgus macaque with 3 million years of divergence and a separate reference genome.

We profiled the transcriptomes of a total of 19,296 high-quality nuclei (6,045 in macaque, 9,297 in marmoset, and 2,679 in mouse), and identified endometrial epithelial cell populations based on documented marker expression and comparison to the human data (Fig. S5; Methods). We confirmed that human endometrial epithelial cells display pervasive expression of *LIF* during the secretory phase (Fig. 4A), with respectively 56%, 62% and 61% of glandular, luminal and ciliated cells expressing *LIF* (average normalised expression: 330 CPM; Fig. 4B). *LIF* expression was also detected at lower levels in immune, endothelial and stromal cells in human (Fig. S6). In the mouse endometrium, epithelial cells represent a smaller population, consistent with other single-cell uterine datasets available for this species (Han et al. 2018; Winkler et al. 2024). While *LIF* expression was not as widespread as in human, mouse glandular epithelial cells expressed *LIF* at relatively high levels, with 17% of cells detected as *LIF*-positive and an average normalised expression of 97 CPM across the glandular cell cluster (Fig. 4A-B). This confirms that a population of mouse endometrial epithelial cells expresses *LIF* in vivo at the end of the luteal phase, which corresponds to the beginning of the window of implantation in this species.

In contrast, *LIF* expression was not detected in rhesus macaque cells and in fewer than 2% of marmoset epithelial cells, despite lenient expression cutoffs (Fig. 4A-B; Methods). These results further support that *LIF*-mediated signalling in the luteal phase has significantly changed during primate evolution, and is not triggered by maternal ovarian hormones alone in either a New World or an Old World monkey with superficial embryonic implantation. We also investigated the expression of *CDA* and *IGFBP7*, but found that these genes are expressed in marmoset epithelial cells similarly to human and mouse, suggesting that their low expression in macaque cells is specific to that species or clade and likely unrelated to implantation phenotypes (Fig. S7).

Finally, we investigated whether the list of candidate genes of interest identified in Fig. 3D also displays convergent expression in human and mouse in vivo (Fig. 4C). Indeed, cell type clustering based on the expression of these candidate genes groups human and mouse epithelial cells together,

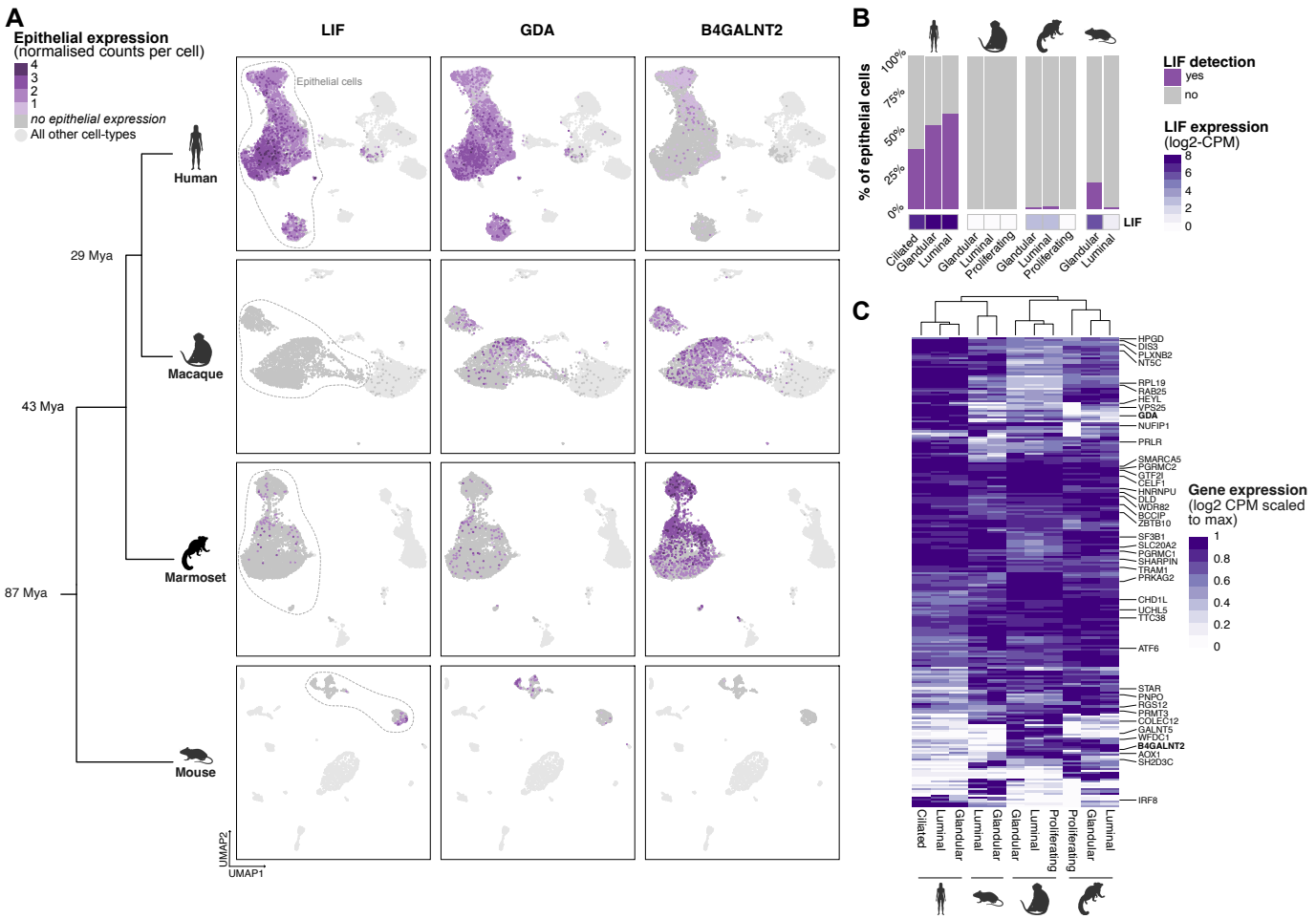

Figure 4: Single-nuclei RNA-seq across primates confirms a convergent evolution of expression patterns for *LIF* and other maternal implantation genes in human and mouse endometrium in vivo during the luteal phase. (A) Uniform manifold approximation and projection (UMAP) of single-nucleus RNA-seq data of mid-luteal phase endometrium from human, macaque, marmoset and mouse. Gene expression values for *LIF*, *GDA* and *B4GALNT2* correspond to normalised counts by nucleus (log2 normalised, scaled) and are represented for epithelial cells only. Other cell types are coloured in light grey regardless of *LIF* expression. **(B)** Quantitative expression of *LIF* across epithelial cell subpopulations is assessed by (top) the proportion of cells with detectable *LIF* expression (>0 normalised counts) and (bottom) pseudo-bulk average expression of *LIF* across all cells in each subpopulation. **(C)** Expression of 232 one-to-one orthologous genes strongly co-expressed with *LIF* across epithelial cell subpopulations in each species (out of 352 candidates; 120 genes did not have a one-to-one ortholog in marmoset). Normalised pseudo-bulk expression values were log2-transformed and scaled to the maximum expression for each gene for representation. Hierarchical clustering was performed based on Euclidean distance of log2-transformed gene expression values. Labelled genes have documented roles in endometrial receptivity, decidualization, embryo implantation, pregnancy outcomes and ovarian hormone response.

and apart from macaque and marmoset. This in vivo comparative analysis therefore confirms that a network of hundreds of co-expressed genes, including *LIF*, have experienced coordinated changes in endometrial epithelial cells resulting in similar expression in human and mouse, and illuminates how deep interstitial implantation phenotypes may have convergently evolved at the functional level. Of these, we highlight *GDA* (glycodelyn) and *B4GALNT2* as two other genes of particular interest with different expression patterns in human and mouse versus macaque and marmoset, both in organoids and in vivo (Fig. 4A, S8). GDA is a glycoprotein secreted by human endometrial epithelial cells during the mid-secretory phase (Mylonas et al. 2006; Seppälä et al. 2002; Stavreus-Evers et al. 2006), and is a recognized biomarker for uterine receptivity in humans (Focarelli et al. 2018). In vitro studies suggest that *GDA* is a key maternal factor that modulates trophoblast invasiveness (Uchida et al. 2013) by enhancing the motility of endometrial cell lineages (Uchida et al. 2007) and reducing the adhesion of chorionic cells (Lam et al. 2011). *B4GALNT2* mediates the catalysis of Sd(a), an important blood antigen also expressed at the surface of epithelial cells and recognized by the DBA lectin. *B4GALNT2* has previously been implicated as an essential actor of embryo recognition and attachment (P.-T. Li et al. 2011; 2012), and can be expressed either maternally or embryonically in different mammalian species (P.-T. Li et al. 2012; Xie et al. 2023; Clark 2015).

Conclusion

In conclusion, this study provides the first evidence for molecular convergence of endometrial epithelial cell transcriptomes during the evolution of interstitial implantation in apes and rodents. Our results illustrate how inter-species transcriptome comparisons combining in vitro and in vivo approaches can inform the molecular tenets of phenotypic change and convergent evolution. This approach is especially important for rapidly evolving traits, such as reproductive phenotypes, where comparisons between pairs of model species such as human and mouse may not be sufficient to

capture functionally relevant change. We anticipate that mechanistic studies dissecting how the molecular actors identified here interact and control maternal-foetal communication will further illuminate how endometrial epithelial cells have evolved to modulate embryonic implantation in mammals.

Materials and Methods

Macaque tissue sampling

Macaque experiments were approved by the CEEA35 Ethical Committee (ethical approval number APAFIS#19437-2019022515049585) for two individuals and by the Paris-Saclay Ethical Committee (ethical approval number APAFIS#20525-2019050616506478) for the third one. Macaca fascicularis females aged between 8 and 13 years were used for this study. For two animals, endometrial biopsies were collected with a Novak curette (1 or 2 mm; GCCI medical: 70-5902-01, 70-5902-02) by vaginal route under ultrasound control and under general anaesthesia. One was menstruating (day 2 of the menstrual cycle) and the other was in luteal phase (day 25 of the menstrual cycle). For the third individual, half of the uterus was opportunistically collected during the euthanasia of a control animal in an unrelated study. Cycle phase was unknown for this animal. The uterine mucosa was separated from the myometrium by scalpel scraping. For all three animals, endometrial fragments were preserved in tissue storage solution (MACS Tissue Storage Solution, Miltenyi Biotec, 130-100-008) with 1% antibiotics (Penicillin/Streptomycin, Gibco, 15140-148) at 4°C for 24 hours prior to generation of the organoid lines.

Mouse tissue sampling

Mice experiments were approved by the Pasteur Institute Ethical Committee (dha220002 – EvoMens). Female mice aged between 10 and 32 weeks were used for this study. We used genetically diverse mice from the Collaborative Cross (CC012, CC042 and CC002 strains, one individual each) to approximate the genetic diversity of our other two study species, which are outbred. Mice were kept in the Pasteur Institute animal housing facility at constant temperature, humidity and day/night cycle, with access to water and food ad libitum. Mice were euthanized by cervical dislocation during estrus, and the whole uterus was used for organoid generation. Organoid cultures were immediately established.

Endometrial epithelial organoid cultures

All cell culture steps were identical between macaque and mouse organoids, except for minor differences in growth media composition as previously published between human and mouse (Boretto et al. 2017; 2019; Margherita Y. Turco et al. 2017) (Table S5, S6).

Macaque endometrial biopsies or mouse uterine horns were rinsed with DPBS without Ca2+/Mg2+ (Gibco, 14190144), and cut into small pieces with dissecting scissors in a Petri dish containing 200 ul of ice-cold DMEMF12 (Gibco, 12634-010) on ice. Tissue samples were transferred to a C-tube (Miltenyi Biotec, 130-093-237) and both enzymatically and mechanically dissociated in 8 ml of Liver Digest Medium (Gibco, 17703034) containing 1% antibiotics (Penicillin/Streptomycin, Gibco, 15140-148) using a GentleMacs tissue dissociator (Miltenyi Biotec, 130-096-427) on manufacturer's program Multi_B01 at 37°C. Tissue dissociation was completed by syringe trituration, passing the solution through 18G and 21G needles, 10 times each. Digestion was stopped with ice-cold DMEMF12 and the supernatant was sequentially filtered through a 100 µm cell strainer (Falcon, 352360) and a 30 µm cell strainer (Miltenyi Biotec, 130-098-458). The fraction retained above the 30 µm filter, containing mainly undigested or partially digested glands, was recovered. Both fractions (cells and glands larger than 30 um, and cells smaller than 30 µm including digested glands) were centrifuged 10 min at 300g at 4°C. Both pellets were resuspended in ice-cold 80% Matrigel (Corning, Growth Factor Reduced, 356231)/20% DMEMF12 (Gibco, 12634-010) at 1:20 ratio (vol/vol), and 25 µl droplets were plated in pre-warmed 48-well plates (Corning, 3548). After solidification, 250 µl of growth medium were added in each well (Table S5 for growth media composition for mouse, and Table S6 for macaque). Medium was refreshed every 2 to 3 days. Organoid cultures were passaged every 8 to 12 days by manual pipetting at a ratio of 1:3 to 1:5 depending on growth efficiency. From the first passage, the cultures from the fractions above 30 µm and below 30 µm were pooled. Organoids of low passage number (P1 – P3) were used for all experiments.

Organoid hormonal treatment

Mouse and macaque endometrial epithelial organoids were treated for two consecutive days with 17-ß estradiol (E2) (Sigma Aldrich, E8875) at 10 nM or for two days with 17-ß estradiol (E2) (Sigma Aldrich, E8875) at the same concentration following by two days with progesterone (P4) (Sigma Aldrich, P8783) at 1µM. At the end of each experiment, endometrial organoids were removed from Matrigel with 250 µl of Cell Recovery Solution (Corning, 354253) per well (1h at 4°C) and centrifuged at 400g for 10 min at 4°C. Fixations for immunochemistry and immunofluorescence were performed immediately, as detailed below. Before RNA extraction, the organoids were cryopreserved in Recovery™-Cell Culture Freezing Medium (Gibco, 12648010) and stored at -80°C in a Mr. Frosty™ freezing container (Thermo Fisher, 5100-0001) for 24 hours and then in liquid nitrogen.

Immunofluorescence and confocal microscopy

Organoids were fixed for 30 min in formalin (Roth, P087.5) at room temperature, centrifuged and the organoid pellet resuspended in 70% ethanol. Organoids were permeabilized using PBSFT (FBS 10% (Gibco, 10270-106) and Triton X100 0,5% (Sigma Aldrich, 9036-19-5) in DPBS (Gibco, 14190144)), which was also used as incubating and rinsing solvent during the immunostaining process. Primary antibodies were incubated overnight at 4°C (Table S7 for a detailed list of antibodies). Organoids were centrifuged at 300g for 10 min at 4°C and washed twice with PBSFT. Secondary antibodies were incubated overnight at 4°C (all from Novus Biologicals: DyLight 488 donkey anti-mouse IgG (NBP1-75125) or DyLight 650 donkey anti-rabbit IgG (NBP1-75644) at 1:200 and DAPI (Invitrogen, R73606)). Final rinsing was done with DPBS (Gibco, 14190144) and immunostained organoids were placed in a 96-well flat bottom plate (Corning, 3474), in 100 µl of DBPS (Gibco, 14190144). Immunofluorescence microscopy was performed on a Nikon eclipse Ti2, CSU-W1 confocal microscope, using x20 or x40 lenses and NIS elements AR, software v.5.11.02.

Immunohistochemistry and Periodic Acid Schiff staining

After removing the growth medium, organoids were removed from the Matrigel as above, embedded in 4% agarose (Sigma, A9639), fixed overnight in formalin at 4°C, dehydrated and paraffin wax-embedded. Sections of 3 µm were subjected to immunohistochemical staining for ESR1, PGR and acetyl-α tubulin (Table S7 for antibodies used). Antigen retrieval was performed with a citrate buffer at pH6 for PGR and acetyl-α tubulin, and Tris EDTA buffer at pH9 for ESR1, at 100°C for 20 min. This was followed by detection with streptavidin-HRP-conjugated secondary antibodies (LEICA, Bond Intense R Detection System, DS9263). Sections were counterstained with haematoxylin (Sigma, GHS2128) for 5 min, dehydrated and mounted. Negative controls were performed using mouse and rabbit sera (1/1000, Jackson ImmunoResearch, 015-000-120 and 011-000-120) as recommended by The Histochemical Society's Standards of Practice for Validation of Immunohistochemical Assays (Hewitt et al. 2014). Periodic Acid Schiff (PAS) staining was performed to visualise mucin. Paraffin sections were dewaxed, rehydrated and immersed in 1% periodic acid (Sigma, P7875) for 7 min, rinsed in water, treated in Schiff's reagent (Sigma, 1.09033.0500) for 20 min, rinsed in water, counterstained with Harris haematoxylin (Sigma, GHS2128) for 1 min, washed, immersed in a saturated solution of lithium carbonate (Sigma, 62470-500G-F), washed, dehydrated and mounted. Pictures were taken using a ZEISS Zen.Apotome.2-upright widefield microscope at x40 magnification and Zen blue 2012 imaging software.

Organoid size measurements

Organoid size was assessed by measuring the largest axis. For each condition, measurements were made at day 5, 7 and 9 on all organoids present in the same plane of two images taken randomly in two different wells. Pictures were taken using an Olympus CKX53 microscope at x10 magnification and analysed with ImageJ software. Organoid sizes were compared using 1-way analysis of variance (ANOVA). This experiment was performed across 3 biological replicates for each condition.

RNA extraction and quality assessment

This experiment was performed as triplicates, with the exception of the E2+P4 experiment in mouse, where only two duplicates were successfully extracted. RNA was extracted from organoids using the RNeasy® Plus Micro Kit with on column DNAse treatment (Qiagen, 74034) according to the manufacturer's instructions. RNA quality and quantity were assessed using Agilent RNA nano or pico chips on a Agilent BioAnalyzer 2100 and a Qubit with Qubit RNA HS Assay Kit (Thermo Fischer, Q32852), respectively (Table S8).

Bulk RNA-seq library preparation and sequencing

Library preparations were prepared using the Illumina® Stranded mRNA prep, ligation kit (Illumina, 20040532) according to the manufacturer's instruction from 35 ng of RNA (except for macaque replicate_2, for which 5 ng were used for all experimental conditions). Library concentrations were assessed using a Qubit instrument with dsDNA HS Assay (Thermo Fischer, Q32854), and library fragment sizes were assessed using Agilent High Sensitivity DNA chips on an Agilent BioAnalyzer 2100 instrument. Equimolar pools of 8 libraries including one replicate of each condition and species were sequenced with NextSeq 1000/2000 P2 reagents 100 cycles kit using an Illumina NextSeq2000 instrument. Libraries were sequenced as single-end 108 bp reads with an average library size of 62 millions reads (Table S8).

Human organoid data curation

We curated publicly available data from two equivalent experiments in human organoids, which were stimulated with E2 and P4 over a similar timecourse (Fitzgerald et al. 2019; Garcia-Alonso et al. 2021). The first dataset was sequenced as bulk transcriptomes using Illumina paired-end reads, while the second was sequenced as single cells using 10XGenomics Chromium GEX library preparation and Illumina sequencing. Both of those works included both biological and technical replicates, and we only extracted one technical replicate per biological sample. In total, the human dataset consists of 7 controls, 3 E2 treatments and 7 E2+P4 treatments. Of note, some E2+P4 samples were also treated with cAMP, a stromal decidualization factor; however, transcriptomic analyses revealed that those samples grouped with other E2+P4 samples and that cAMP treatment had little impact on the transcriptome, so we elected to retain those as well.

Transcriptome analysis of organoid experiments

Reference transcriptomes

The reference transcriptomes for human (GRCh38.p13), crab-eating macaque (Macaca_fascicularis_6.0), and mouse (GRCm39) were downloaded from Ensembl 108 (Cunningham et al. 2022).

Orthologous gene selection

To perform cross-species comparisons, we extracted one-to-one orthologous protein coding genes present in all three species (human, mouse and crab-eating macaque) using Ensembl Biomart 108, resulting in 15,015 genes.

Bulk RNA sequencing analysis

Quality of bulk RNA-seq libraries, produced for this study and from published data, was controlled using FastQC v.0.11.9. Low quality bases and adapters were removed using Trimmomatic v.039 (Bolger, Lohse, and Usadel 2014). Trimmed reads were pseudo-mapped using Salmon 1.9.0 (Patro et al. 2017) to the appropriate reference transcriptome. Quality control statistics were extracted from the report generated by Salmon during mapping. Transcript quantifications were converted into gene quantifications using tximport 1.24.0 (Soneson, Love, and Robinson 2015).

Reanalysis of published human organoid single-cell transcriptomes

For single-cell RNA-seq data from human organoids, we followed the standard mapping procedure of 10xGenomics CellRanger 6.0.1 (Zheng et al. 2017) to the reference human transcriptome. The output was processed in Seurat 4.2.0 (Hao et al. 2021). Cells were retained if they met the following quality criteria: a minimum of 250 genes were detected (nFeature_RNA), a minimum of 500 unique molecules detected (nCount_RNA), a log10 of number of genes per UMI (log10GenesPerUMI) higher than 0.80, and fewer than 20% of mitochondrial reads. After removing low quality cells, gene expression was aggregated and extracted as pseudo-bulk quantifications (PseudobulkExpression).

Batch effect removal

Gene expression quantification files were combined into count tables per species. Macaque and mouse libraries were corrected for technical batch effects due to sequencing batches using CombatSeq (sva v3.44.0 R package) (Fig S1 A-B) (Zhang, Parmigiani, and Johnson 2020). Human libraries were corrected for technical batch effects due to sample origin.

Differential expression

Differential expression analysis was performed using DeApp v.1.7.4 (Y. Li and Andrade 2017). Only genes with expression levels over 1 CPM in at least two samples were considered as expressed and retained for analysis. DeApp performs differential expression using DeSeq2 v.1.38.2 (Love, Huber, and Anders 2014), edgeR v. 3.38.4 (Robinson, McCarthy, and Smyth 2010) and limma v. 3.52.4 (Ritchie et al. 2015). Genes were considered as differentially expressed if they have an adjusted p-value below 0.05 for all three methods. Volcano plots shown in Fig. 1 and S2 were constructed using the statistics obtained with limma. We note that statistics obtained across all three methods were highly consistent (Spearman correlation between log fold-change of 0.95) and method choice did not alter the general conclusions.

Cross-species analysis

Transcriptome correlation

Expression counts for the 15,015 one-to-one orthologs were normalised across species using edgeR size factors. Transcriptome correlation was performed on all one-to-one orthologs using log2-transformed normalised expression counts. Mean Spearman correlation coefficient across conditions and species were represented using the R packages stats v.4.2.2 and pheatmap v. 1.0.12. Principal component analysis (PCA) was performed on log2-transformed and z-normalised expression counts using R package FactoMineR v. 2.6.

Cross-species differentially expressed genes

We compared changes in gene expression in response to hormones across species. For each species, DEGs were restricted to one-to-one orthologous genes and intersected across species for each treatment independently. We tested the significance of the intersection across species by performing a hypergeometric test with Benjamini-Hochberg (B-H) p-value adjustment.

Functional enrichment

Functional enrichment analysis was performed with ShinyGO v. 0.77 (Ge, Jung, and Yao 2020) using the Human Hallmark gene set annotations (Liberzon et al. 2015). We used sets of shared DEGs for each combination of species as foreground to perform functional enrichment analysis. Background genes were set to the 13,008 orthologous genes expressed more than 1 CPM in at least two samples for each species (e.g. all genes that have been tested for differential expression in all three species).

Curation of maternal implantation gene set

We manually curated a list of maternally expressed genes with described roles in endometrial receptivity or embryo implantation from recent reviews (Evans et al. 2020; Bazer et al. 2011) and research articles on implantation mechanisms (Table S3). Genes were included when they were expressed in endometrial epithelial cells during the window of implantation and if they were experimentally associated with implantation and endometrial receptivity in at least two independent studies (Table S3).

Gene expression fold-change correlations

Expression fold-change values between treatments and controls were calculated with limma for all one-to-one orthologous genes in the over-represented Hallmark gene sets and in the maternal implantation gene set. Spearman correlations of log-fold-change values were calculated for each gene set between species and conditions. Correlation p-values were adjusted for multiple testing using Benjamini-Hochberg correction. Because we considered a fairly large number of pathways, each containing a relatively small number of genes, we used a relaxed significance threshold for this analysis (adjusted p-value < 0.1).

Gene co-expression analysis

Co-expression analysis across species and conditions was performed on the one-to-one orthologs genes using the WGCNA v.1.71 (Langfelder and Horvath 2008) R package. The weighted gene co-expression network was constructed using as input edgeR factor-scaled log2 RPKM expression levels for the three species in the treated samples and a soft thresholding power (β) of 6, resulting in 13 co-expression gene modules (Fig. S4). Genes with a co-expression weight with *LIF* higher than 0.4 were considered as candidates of interest for further analysis.

Single-nuclei RNA-seq

Tissue collection

A half snap-frozen uterus in mid-luteal phase from a female rhesus macaque individual (Macaca mulatta) was sourced from the Biomedical Primate Research Center (BPRC) biobank. All procedures regarding the maintenance of the Tissue bank at BPRC were in accordance with the Dutch law on animals, and the European legislation concerning the care and use of laboratory animals. The BPRC is accredited by the American Association for Accreditation of Laboratory Animal Care (AAALAC) International and is compliant with the European directive 2010/63/EU as well as the "Standard for Humane Care and Use of Laboratory Animals by Foreign Institutions" (National Institutes of Health, ID A5539-01). Cycle phase was confirmed histologically by an experienced veterinary pathologist. Thin cryostat organ sections were obtained and the endometrial part of the tissue

was identified by hematoxylin eosin staining and dissected on serial sections with a cold scalpel before processing.

A whole uterus in mid-luteal phase was obtained from a female common marmoset individual (Callithrix jacchus) after approval from the CEEA71 Ethical Committee (ethical approval number APAFIS#31395-20210325103447). Cycle phase was determined by plasma progesterone titration by Enzyme Linked Fluorescent Assay (MiniVIDAS® Progesterone 30409, Biomérieux, France) over 15 days prior to surgery, and confirmed histologically after surgery. Hysterectomy was performed under general anaesthesia when progesterone levels plateaued to the maximum levels observed in this species (139,43 ng/uL). The uterus was immediately rinsed with cold PBS 1x and dissected on ice to separate the endometrium from the myometrium. Endometrium samples were snap-frozen in liquid nitrogen and stored at -80°C before processing.

A whole uterus in diestrus was obtained from a female mouse from the Collaborative Cross line CC061. Cycle phase was determined by vaginal smears to identify the diestrus phase and histologically confirmed after sacrifice. In mice, the peak of progesterone occurs during diestrus (McLean et al. 2012). This cycle phase is similar to the late secretory phase in primates. The uterus was immediately rinsed with cold PBS 1x, snap-frozen in liquid nitrogen and stored at -80°C before processing.

Nuclei isolation

For the rhesus macaque sample, all buffers were prepared in agreement with demonstrated protocol CG000375_RevC from 10xGenomics for Complex Tissues for Single Cell Multiome ATAC + Gene Expression Sequencing. A few adaptations were made to the nuclei isolation protocol. Briefly, the endometrial tissue fragments were incubated for 5 min in 2 ml of lysis buffer and homogenised 25 times using a dounce on ice before adding 2 ml of wash buffer. The suspension was filtered through a 100 um filter and centrifuged for 5 min at 500g and 4°C. The pellet was washed a second time with 1 ml of wash buffer. After centrifugation, nuclei were resuspended in 500 µl of wash buffer and labelled with an anti-nuclear pore complex proteins antibody (clone Mab414) and sorted on a FACSAria instrument (BD Biosciences), with a 100 nozzle on a cold block. The collection tube was then cold centrifuged for 7 min at 500g and the nuclei pellet was incubated for 2 min on ice with lysis buffer containing digitonin to permeabilize the membranes. After a final washing step with 1 ml of wash buffer and centrifugation, nuclei were resuspended in 49 µl of diluted nuclei buffer to obtain 12,500 nuclei in 5 µl of buffer for further processing.

For both mouse and marmoset, endometrial samples were embedded in OCT and thinly sliced with a scalpel on ice. The fragments were transferred to a dounce, incubated for 5 min in 1 ml lysis buffer (10mM Tris-HCL pH7.5, 146 mM NaCl, 1 mM CaCl2, 21 mM MgCl2, 0.03% Tween-20, 0.01% BSA, 1 mM DTT, 10% EZ Lysis Buffer (Sigma/Merck), 0.5 U/µl RNase Inhibitor) and then ground with a pestle. The homogenate was then filtered through a 70 um strainer, rinsed with 400 µl of wash buffer (250 mM sucrose, 10mM Tris-HCL pH7.5, 5 mM MgCl2, 1% BSA, 1 mM DTT, 0.5 U/µl RNase Inhibitor) and centrifuged for 5 min at 500g and 4°C. The pellet was washed a second time and centrifuged again. The nuclei pellet was finally resuspended in 200 ul of wash buffer and filtered through a 40 µm filter. 15,000 nuclei were loaded in the 10XGenomics Chromium instrument for each species.

10X Genomics Chromium library preparation and sequencing

For rhesus macaque, nuclei were proceeded immediately with Chromium Next GEM Single Cell Multiome ATAC + Gene Expression Reagent Bundle Kits according to the Chromium Next GEM Single Cell Multiome ATAC + Gene Expression User Guide (CG000338_RevF). For mouse and marmoset, nuclei were proceeded immediately with Chromium Next GEM Single Cell 3′ Kit v3.1 according to Chromium Next GEM Single Cell 3′ Reagent Kits v3.1 (Dual Index) User Guide (CG000315_RevE). Equimolar pools of 4 libraries including one replicate of each species were sequenced with NextSeq 1000/2000 P2 reagents 100 cycles kit using an Illumina NextSeq2000 instrument. Libraries were sequenced as paired-end following the instructions specific to each 10xGenomics chemistry (Multiome or Gene Expression). Equimolar pools including one replicate of each condition and species were sequenced using an Illumina NextSeq2000 instrument.

Raw reads processing

For macaque, mouse and marmoset, CellRanger v.7.1.0 was used for demultiplexing with the corresponding Chromium chemistry. CellRanger transcriptome files were built using mkref function and with the default parameters for each species using the respective genome assemblies (rheMac10, mm10, calJac4). CellRanger count function was used for the generation of the count matrix using the intronic mode (--include-introns) and default parameters to map reads to the transcriptome and generate a count matrix for every UMI. CellRanger prefiltered count matrices (filtered_feature_bc_matrix) without empty droplets were used for downstream analysis.

Nuclei quality filters and data processing

Quality control was performed for each sample independently using Seurat v.4.3 (Hao et al. 2021). SoupX v.1.6.2 (Young and Behjati 2020) correction was applied following standard recommendations to correct the count matrix for ambient RNA contamination. Nuclei expressing fewer than 500 genes, more than 5000 genes and/or more than 5% of mitochondrial reads after SoupX correction were filtered out as low quality. Doublet identification and removal was performed using DoubletFinder v 2.0.3 (McGinnis, Murrow, and Gartner 2019) following standard guidelines (pK auto-estimated, pN=0.25, N=15000 corresponding to the expected number of nuclei loaded during library preparation). Normalisation, feature selection, scaling and dimension reduction was performed using standard procedures with Seurat. Clustering was then performed using the Louvain algorithm and following Seurat guidelines (Hao et al. 2021). Epithelial cell clusters were identified using expression of canonical epithelial markers (EPCAM, CDH1, SOX17), and further refined for the glandular, luminal, ciliated and proliferating epithelial clusters using marker genes from the Human Reproductive Cell Atlas (Garcia-Alonso et al. 2021) and analysis of the top 5 marker genes by cluster (FindAllMarkers with min.pct=0.25, logfc.threshold=0.1; Table S10-11-12 for top marker genes by cluster per species). Other broad endometrial cell types were also identified across all species (Fig. S5). Note that ciliated epithelial cells were not confidently identified in mouse, which may be due to the lower fraction of epithelial cells in this species and therefore lower resolution to detect cell subpopulations.

Finally, depth-normalised pseudo-bulk expression levels were extracted for all epithelial clusters (AggregateExpression). Epithelial clusters expression levels are presented as log2-transformed CPM for the one-to-one orthologous genes of interest.

Human single-cell dataset curation

Human endometrial single-cell RNA-seq data was obtained pre-processed and annotated from the Human Reproductive Cell Atlas. Only samples corresponding to mid-secretory and mid-late-secretory phases were retained to match the time point in the other species. Cell filtering and clustering was performed using the same standards as described above.

References

Altmäe, Signe, Mariann Koel, Urmo Võsa, Priit Adler, Marina Suhorutšenko, Triin Laisk-Podar, Viktorija Kukushkina, et al. 2017. 'Meta-Signature of Human Endometrial Receptivity: A Meta-Analysis and Validation Study of Transcriptomic Biomarkers'. Scientific Reports 7 (August): 10077. https://doi.org/10.1038/s41598-017-10098-3.

Bazer, Fuller W., Guoyao Wu, Greg A. Johnson, Jinyoung Kim, and Gwonhwa Song. 2011. 'Uterine Histotroph and Conceptus Development: Select Nutrients and Secreted Phosphoprotein 1 Affect Mechanistic Target of Rapamycin Cell Signaling in Ewes'. Biology of Reproduction 85 (6): 1094–1107. https://doi.org/10.1095/biolreprod.111.094722.

Bolger, Anthony M., Marc Lohse, and Bjoern Usadel. 2014. 'Trimmomatic: A Flexible Trimmer for Illumina Sequence Data'. Bioinformatics 30 (15): 2114–20. https://doi.org/10.1093/bioinformatics/btu170.

Boretto, Matteo, Benoit Cox, Manuel Noben, Nikolai Hendriks, Amelie Fassbender, Heleen Roose, Frédéric Amant, et al. 2017. 'Development of Organoids from Mouse and Human Endometrium Showing Endometrial Epithelium Physiology and Long-Term Expandability'. Development 144 (10): 1775–86. https://doi.org/10.1242/dev.148478.

Boretto, Matteo, Nina Maenhoudt, Xinlong Luo, Aurélie Hennes, Bram Boeckx, Bich Bui, Ruben Heremans, et al. 2019. 'Patient-Derived Organoids from Endometrial Disease Capture Clinical Heterogeneity and Are Amenable to Drug Screening'. Nature Cell Biology 21 (8): 1041–51. https://doi.org/10.1038/s41556-019-0360-z.

Carter, Anthony M., and Allen C. Enders. 2004. 'Comparative Aspects of Trophoblast Development and Placentation'. Reproductive Biology and Endocrinology 2 (1): 46. https://doi.org/10.1186/1477-7827-2-46.

Cha, Jeeyeon, Xiaofei Sun, and Sudhansu K. Dey. 2012. 'Mechanisms of Implantation: Strategies for Successful Pregnancy'. Nature Medicine 18 (12): 1754–67. https://doi.org/10.1038/nm.3012.

Clark, Gary F. 2015. 'Functional Glycosylation in the Human and Mammalian Uterus'. Fertility Research and Practice 1 (1): 17. https://doi.org/10.1186/s40738-015-0007-0.

Critchley, Hilary O. D., Jacqueline A. Maybin, Gregory M. Armstrong, and Alistair R. W. Williams. 2020. 'Physiology of the Endometrium and Regulation of Menstruation'. Physiological Reviews 100 (3): 1149–79. https://doi.org/10.1152/physrev.00031.2019.

Cunningham, Fiona, James E. Allen, Jamie Allen, Jorge Alvarez-Jarreta, M. Ridwan Amode, Irina M. Armean, Olanrewaju Austine-Orimoloye, et al. 2022. 'Ensembl 2022'. Nucleic Acids Research 50 (D1): D988–95. https://doi.org/10.1093/nar/gkab1049.

Díaz-Gimeno, Patricia, José A. Horcajadas, José A. Martínez-Conejero, Francisco J. Esteban, Pilar Alamá, Antonio Pellicer, and Carlos Simón. 2011. 'A Genomic Diagnostic Tool for Human Endometrial Receptivity Based on the Transcriptomic Signature'. Fertility and Sterility 95 (1): 50–60, 60.e1-15. https://doi.org/10.1016/j.fertnstert.2010.04.063.

Domínguez, F., J. Remohí, A. Pellicer, and C. Simón. 2003. 'Human Endometrial Receptivity: A Genomic Approach'. Reproductive Biomedicine Online 6 (3): 332–38. https://doi.org/10.1016/s1472-6483(10)61853-6.

Enders, A. C., and A. Lopata. 1999. 'Implantation in the Marmoset Monkey: Expansion of the Early Implantation Site'. The Anatomical Record 256 (3): 279–99. https://doi.org/10.1002/(SICI)1097-0185(19991101)256:3<279::AID-AR7>3.0.CO;2-O.

Erkenbrack, Eric M., Jamie D. Maziarz, Oliver W. Griffith, Cong Liang, Arun R. Chavan, Mauris C. Nnamani, and Günter P. Wagner. 2018. 'The Mammalian Decidual Cell Evolved from a Cellular Stress Response'. PLOS Biology 16 (8): e2005594. https://doi.org/10.1371/journal.pbio.2005594.

Evans, Jemma, Jennifer Hutchison, Lois A. Salamonsen, and David W. Greening. 2020. 'Proteomic Insights into Endometrial Receptivity and Embryo-Endometrial Epithelium Interaction for Implantation Reveal Critical Determinants of Fertility'. Proteomics 20 (1): e1900250. https://doi.org/10.1002/pmic.201900250.

Fainboim, L., and L. Arruvito. 2011. 'Mechanisms Involved in the Expansion of Tregs during Pregnancy: Role of IL-2/STAT5 Signalling'. Journal of Reproductive Immunology 88 (2): 93–98. https://doi.org/10.1016/j.jri.2010.12.007.

Fernando, S. C., J. S. Buck, M. D. Ashworth, J. W. Ross, R. D. Geisert, and U. DeSilva. 2006. 'Porcine Endometrial and Conceptus Tissue Kallikrein 1, 4, 11, and 14 Gene Expression'. Reproduction (Cambridge, England) 132 (6): 939–47. https://doi.org/10.1530/rep.1.01013.

Filant, Justyna, and Thomas E. Spencer. 2013. 'Endometrial Glands Are Essential for Blastocyst Implantation and Decidualization in the Mouse Uterus'. Biology of Reproduction 88 (4): 93. https://doi.org/10.1095/biolreprod.113.107631.

Finkenzeller, Daniela, Beate Fischer, Sabine Lutz, Heinrich Schrewe, Takehiko Shimizu, and Wolfgang Zimmermann. 2003. 'Carcinoembryonic Antigen-Related Cell Adhesion Molecule 10 Expressed Specifically Early in Pregnancy in the Decidua Is Dispensable for Normal Murine Development'. Molecular and Cellular Biology 23 (1): 272–79. https://doi.org/10.1128/MCB.23.1.272-279.2003.

Fitzgerald, Harriet C., Pramod Dhakal, Susanta K. Behura, Danny J. Schust, and Thomas E. Spencer. 2019. 'Self-Renewing Endometrial Epithelial Organoids of the Human Uterus'. Proceedings of the National Academy of Sciences of the United States of America 116 (46): 23132–42. https://doi.org/10.1073/pnas.1915389116.

Focarelli, Riccardo, Alice Luddi, Vincenzo De Leo, Angela Capaldo, Anita Stendardi, Valentina Pavone, Linda Benincasa, Giuseppe Belmonte, Felice Petraglia, and Paola Piomboni. 2018. 'Dysregulation of GdA Expression in Endometrium of Women With Endometriosis: Implication for Endometrial Receptivity'. Reproductive Sciences (Thousand Oaks, Calif.) 25 (4): 579–86. https://doi.org/10.1177/1933719117718276.

Forde, N., M.E. Beltman, G.B. Duffy, P. Duffy, J.P. Mehta, P. Ó'Gaora, J.F. Roche, P. Lonergan, and M.A. Crowe. 2011. 'Changes in the Endometrial Transcriptome During the Bovine Estrous Cycle: Effect of Low Circulating Progesterone and Consequences for Conceptus Elongation1'. Biology of Reproduction 84 (2): 266–78. https://doi.org/10.1095/biolreprod.110.085910.

Garcia-Alonso, Luz, Louis-François Handfield, Kenny Roberts, Konstantina Nikolakopoulou, Ridma C. Fernando, Lucy Gardner, Benjamin Woodhams, et al. 2021. 'Mapping the Temporal and Spatial Dynamics of the Human Endometrium in Vivo and in Vitro'. Nature Genetics 53 (12): 1698–1711. https://doi.org/10.1038/s41588-021-00972-2.

Garrido-Gomez, Tamara, Nerea Castillo-Marco, Mónica Clemente-Ciscar, Teresa Cordero, Irene Muñoz-Blat, Alicia Amadoz, Jorge Jimenez-Almazan, et al. 2021. 'Disrupted PGR-B and ESR1 Signaling Underlies Defective Decidualization Linked to Severe Preeclampsia'. Edited by Bérénice A Benayoun and Kathryn Song Eng Cheah. eLife 10 (October): e70753. https://doi.org/10.7554/eLife.70753.

Garrido-Gomez, Tamara, Katherine Ona, Mirhan Kapidzic, Matthew Gormley, Carlos Simón, Olga Genbacev, and Susan J. Fisher. 2017. 'Severe Pre-Eclampsia Is Associated with Alterations in Cytotrophoblasts of the Smooth Chorion'. Development (Cambridge, England) 144 (5): 767–77. https://doi.org/10.1242/dev.146100.

Ge, Steven Xijin, Dongmin Jung, and Runan Yao. 2020. 'ShinyGO: A Graphical Gene-Set Enrichment Tool for Animals and Plants'. Bioinformatics (Oxford, England) 36 (8): 2628–29. https://doi.org/10.1093/bioinformatics/btz931.

Gleeson, N., M. Jordan, B. Sheppard, and J. Bonnar. 1993. 'Cyclical Variation in Endometrial Oestrogen and Progesterone Receptors in Women with Normal Menstruation and Dysfunctional Uterine Bleeding'. European Journal of Obstetrics, Gynecology, and Reproductive Biology 48 (3): 207–14. https://doi.org/10.1016/0028-2243(93)90089-u.

Han, Xiaoping, Renying Wang, Yincong Zhou, Lijiang Fei, Huiyu Sun, Shujing Lai, Assieh Saadatpour, et al. 2018. 'Mapping the Mouse Cell Atlas by Microwell-Seq'. Cell 172 (5): 1091-1107.e17. https://doi.org/10.1016/j.cell.2018.02.001.

Hao, Yuhan, Stephanie Hao, Erica Andersen-Nissen, William M. Mauck, Shiwei Zheng, Andrew Butler, Maddie J. Lee, et al. 2021. 'Integrated Analysis of Multimodal Single-Cell Data'. Cell 184 (13): 3573-3587.e29. https://doi.org/10.1016/j.cell.2021.04.048.

Hewitt, Stephen M., Denis G. Baskin, Charles W. Frevert, William L. Stahl, and Eduardo Rosa-Molinar. 2014. 'Controls for Immunohistochemistry: The Histochemical Society's Standards of Practice for Validation of Immunohistochemical Assays'. The Journal of Histochemistry and Cytochemistry: Official Journal of the Histochemistry Society 62 (10): 693–97. https://doi.org/10.1369/0022155414545224.

Hu, Wenwei, Zhaohui Feng, Angelika K. Teresky, and Arnold J. Levine. 2007. 'P53 Regulates Maternal Reproduction through LIF'. Nature 450 (7170): 721–24. https://doi.org/10.1038/nature05993.

Huchard, Elise, Alexandre Courtiol, Julio A. Benavides, Leslie A. Knapp, Michel Raymond, and Guy Cowlishaw. 2009. 'Can Fertility Signals Lead to Quality Signals? Insights from the Evolution of Primate Sexual Swellings'. Proceedings of the Royal Society B: Biological Sciences 276 (1663): 1889–97. https://doi.org/10.1098/rspb.2008.1923.

Kang, Hey-Joo, and Zev Rosenwaks. 2018. 'P53 and Reproduction'. Fertility and Sterility 109 (1): 39–43. https://doi.org/10.1016/j.fertnstert.2017.11.026.

Kaya, Hatice S., Alison M. Hantak, Lisa J. Stubbs, Robert N. Taylor, Indrani C. Bagchi, and Milan K. Bagchi. 2015. 'Roles of Progesterone Receptor A and B Isoforms during Human Endometrial Decidualization'. Molecular Endocrinology (Baltimore, Md.) 29 (6): 882–95. https://doi.org/10.1210/me.2014-1363.

King, Anne E., Hilary OD Critchley, and Rodney W. Kelly. 2003. 'Innate Immune Defences in the Human Endometrium'. Reproductive Biology and Endocrinology 1 (1): 116. https://doi.org/10.1186/1477-7827-1-116.

Kolkova, Z., V. Noskova, A. Ehinger, S. Hansson, and B. Casslén. 2010. 'G Protein-Coupled Estrogen Receptor 1 (GPER, GPR 30) in Normal Human Endometrium and Early Pregnancy Decidua'. Molecular Human Reproduction 16 (10): 743–51. https://doi.org/10.1093/molehr/gaq043.

Kromrey, Sarah A., Paul W. Czoty, and Michael A. Nader. 2015. 'Relationship between Estradiol and Progesterone Concentrations and Cognitive Performance in Normally Cycling Female Cynomolgus Monkeys'. Hormones and Behavior 72 (June): 12–19. https://doi.org/10.1016/j.yhbeh.2015.04.017.

Lam, Kevin K. W., Philip C. N. Chiu, Cheuk-Lun Lee, Ronald T. K. Pang, Carmen O. N. Leung, Hannu Koistinen, Markku Seppala, Pak-Chung Ho, and William S. B. Yeung. 2011. 'Glycodelin-A Protein Interacts with Siglec-6 Protein to Suppress Trophoblast Invasiveness by down-Regulating Extracellular Signal-Regulated Kinase (ERK)/c-Jun

Signaling Pathway'. The Journal of Biological Chemistry 286 (43): 37118–27. https://doi.org/10.1074/jbc.M111.233841.

Lamprianidou, Eleftheria, Michail Daniilidis, Chryssoula Kordella, Emmanouela Zoulia, Evangelia Nakou, Antonios Gerofotis, Athina Vasilaki, George Pantos, and Ioannis Kotsianidis. 2020. 'The STAT Signaling Profile at the Single Cell Level Reveals Novel Insights in the Association of FOXP3+ T Regulatory Cells with Recurrent Spontaneous Abortions before and after Lymphocyte Immunotherapy'. Clinical Immunology 210 (January): 108261. https://doi.org/10.1016/j.clim.2019.108261.

Langfelder, Peter, and Steve Horvath. 2008. 'WGCNA: An R Package for Weighted Correlation Network Analysis'. BMC Bioinformatics 9 (December): 559. https://doi.org/10.1186/1471-2105-9-559.

Li, Pei-Tzu, Chi-Jr Liao, Wen-Guey Wu, Lung-Chi Yu, and Sin Tak Chu. 2011. 'Progesterone-Regulated B4galnt2 Expression Is a Requirement for Embryo Implantation in Mice'. Fertility and Sterility 95 (7): 2404-2409.e3. https://doi.org/10.1016/j.fertnstert.2011.03.043.

Li, Pei-Tzu, Chi-Jr Liao, Lung-Chi Yu, Wen-Guey Wu, and Sin Tak Chu. 2012. 'Localization of B4GALNT2 and Its Role in Mouse Embryo Attachment'. Fertility and Sterility 97 (5): 1206-1212.e1-3. https://doi.org/10.1016/j.fertnstert.2012.02.019.

Li, Q., M. Zhang, S. Kumar, L. J. Zhu, D. Chen, M. K. Bagchi, and I. C. Bagchi. 2001. 'Identification and Implantation Stage-Specific Expression of an Interferon-Alpha-Regulated Gene in Human and Rat Endometrium'. Endocrinology 142 (6): 2390–2400. https://doi.org/10.1210/endo.142.6.8101.

Li, Yan, and Jorge Andrade. 2017. 'DEApp: An Interactive Web Interface for Differential Expression Analysis of next Generation Sequence Data'. Source Code for Biology and Medicine 12: 2. https://doi.org/10.1186/s13029-017-0063-4.

Liberzon, Arthur, Chet Birger, Helga Thorvaldsdóttir, Mahmoud Ghandi, Jill P. Mesirov, and Pablo Tamayo. 2015. 'The Molecular Signatures Database (MSigDB) Hallmark Gene Set Collection'. Cell Systems 1 (6): 417–25. https://doi.org/10.1016/j.cels.2015.12.004.

Liu, Zhen-Kun, Rong-Chun Wang, Bing-Chen Han, Ying Yang, and Jing-Pian Peng. 2012. 'A Novel Role of IGFBP7 in Mouse Uterus: Regulating Uterine Receptivity through Th1/Th2 Lymphocyte Balance and Decidualization'. PloS One 7 (9): e45224. https://doi.org/10.1371/journal.pone.0045224.

Love, Michael I., Wolfgang Huber, and Simon Anders. 2014. 'Moderated Estimation of Fold Change and Dispersion for RNA-Seq Data with DESeq2'. Genome Biology 15 (12): 550. https://doi.org/10.1186/s13059-014-0550-8.

Lundgren, D. W., J. J. Moore, S. M. Chang, P. L. Collins, and A. S. Chang. 1997. 'Gestational Changes in the Uterine Expression of an Inwardly Rectifying K+ Channel, ROMK'. Proceedings of the Society for Experimental Biology and Medicine. Society for Experimental Biology and Medicine (New York, N.Y.) 216 (1): 57–64. https://doi.org/10.3181/00379727-216-44156.

Lynch, Vincent J., Robert D. Leclerc, Gemma May, and Günter P. Wagner. 2011. 'Transposon-Mediated Rewiring of Gene Regulatory Networks Contributed to the Evolution of Pregnancy in Mammals'. Nature Genetics 43 (11): 1154–59. https://doi.org/10.1038/ng.917.

Machado, Diana A., Alejandra E. Ontiveros, and Richard R. Behringer. 2022. 'Chapter Three - Mammalian Uterine Morphogenesis and Variations'. In Current Topics in Developmental Biology, edited by Thomas Gridley and Leif Oxburgh, 148:51–77. Mouse Models of Development and Disease. Academic Press. https://doi.org/10.1016/bs.ctdb.2021.12.004.

Manley, Charisma N., Venkataraman Deepak, Nithin Ravikumar, Alicia K. Smith, Anna K. Knight, Martina L. Badell, Neil Sidell, and Augustine Rajakumar. 2020. 'Transcription Factor AP2A Affects sFLT1 Expression and Decidualization in Decidual Stromal Cells: Implications to Preeclampsia Pathology'. Pregnancy Hypertension 21 (July): 152–58. https://doi.org/10.1016/j.preghy.2020.06.001.

Manohar, Murli, Huma Khan, Vinay Shukla, Vinita Das, Anjoo Agarwal, Amita Pandey, Waseem Siddiqui, and Anila Dwivedi. 2014. 'Proteomics & Bioinformatics Proteomic Identification and Analysis of Human Endometrial Proteins Associated with Unexplained Infertility'. Journal of Proteomics & Bioinformatics 7 (November). https://doi.org/10.4172/jpb.1000340.

Martínez-Aguilar, Rocío, Lucy E. Kershaw, Jane J. Reavey, Hilary O. D. Critchley, and Jacqueline A. Maybin. 2021. 'HYPOXIA AND REPRODUCTIVE HEALTH: The Presence and Role of Hypoxia in the Endometrium'. Reproduction (Cambridge, England) 161 (1): F1–17. https://doi.org/10.1530/REP-20-0268.

McGinnis, Christopher S., Lyndsay M. Murrow, and Zev J. Gartner. 2019. 'DoubletFinder: Doublet Detection in Single-Cell RNA Sequencing Data Using Artificial Nearest Neighbors'. Cell Systems 8 (4): 329-337.e4. https://doi.org/10.1016/j.cels.2019.03.003.

McGowen, Michael R., Offer Erez, Roberto Romero, and Derek E. Wildman. 2014. 'The Evolution of Embryo Implantation'. The International Journal of Developmental Biology 58 (2–4): 155–61. https://doi.org/10.1387/ijdb.140020dw.

McLean, Ashleigh C., Nicolas Valenzuela, Stephen Fai, and Steffany A. L. Bennett. 2012. 'Performing Vaginal Lavage, Crystal Violet Staining, and Vaginal Cytological Evaluation for Mouse Estrous Cycle Staging Identification'. Journal of Visualized Experiments: JoVE, no. 67 (September): e4389. https://doi.org/10.3791/4389.

Mehasseb, Mohamed Khairy, Rina Panchal, Anthony Henry Taylor, Laurence Brown, Stephen Charles Bell, and Marwan Habiba. 2011. 'Estrogen and Progesterone Receptor Isoform Distribution through the Menstrual Cycle in Uteri with and without Adenomyosis'. Fertility and Sterility 95 (7): 2228–35, 2235.e1. https://doi.org/10.1016/j.fertnstert.2011.02.051.

Mika, Katelyn, Camilla M Whittington, Bronwyn M McAllan, and Vincent J Lynch. 2022. 'Gene Expression Phylogenies and Ancestral Transcriptome Reconstruction Resolves Major Transitions in the Origins of Pregnancy'. Edited by Antonis Rokas. eLife 11 (June): e74297. https://doi.org/10.7554/eLife.74297.

Murat, Florent, Noe Mbengue, Sofia Boeg Winge, Timo Trefzer, Evgeny Leushkin, Mari Sepp, Margarida Cardoso-Moreira, et al. 2023. 'The Molecular Evolution of Spermatogenesis across Mammals'. Nature 613 (7943): 308–16. https://doi.org/10.1038/s41586-022-05547-7.

Murphy, Shawn P., Chandrakant Tayade, Ali A. Ashkar, Kota Hatta, Jianhong Zhang, and B. Anne Croy. 2009. 'Interferon Gamma in Successful Pregnancies'. Biology of Reproduction 80 (5): 848–59. https://doi.org/10.1095/biolreprod.108.073353.

Muter, Joanne, Vincent J. Lynch, Rajiv C. McCoy, and Jan J. Brosens. 2023. 'Human Embryo Implantation'. Development 150 (10): dev201507. https://doi.org/10.1242/dev.201507.

Mylonas, Ioannis, Udo Jeschke, Christiane Kunert-Keil, Naim Shabani, Darius Dian, Ingo Bauerfeind, Christina Kuhn, Markus S. Kupka, and Klaus Friese. 2006. 'Glycodelin A Is Expressed Differentially in Normal Human Endometrial Tissue throughout the Menstrual Cycle as Assessed by Immunohistochemistry and in Situ Hybridization'. Fertility and Sterility 86 (5): 1488–97. https://doi.org/10.1016/j.fertnstert.2006.03.062.

Okumu, L. A., T. Fair, J. Szekeres-Bartho, A. M. O'Doherty, M. A. Crowe, J. F. Roche, P. Lonergan, and N. Forde. 2011. 'Endometrial Expression of Progesterone-Induced Blocking Factor and Galectins-1, -3, -9, and -3 Binding Protein in the Luteal Phase and Early Pregnancy in Cattle'. Physiological Genomics 43 (14): 903–10. https://doi.org/10.1152/physiolgenomics.00251.2010.

Patro, Rob, Geet Duggal, Michael I. Love, Rafael A. Irizarry, and Carl Kingsford. 2017. 'Salmon Provides Fast and Bias-Aware Quantification of Transcript Expression'. Nature Methods 14 (4): 417–19. https://doi.org/10.1038/nmeth.4197.

Ritchie, Matthew E., Belinda Phipson, Di Wu, Yifang Hu, Charity W. Law, Wei Shi, and Gordon K. Smyth. 2015. 'Limma Powers Differential Expression Analyses for RNA-Sequencing and Microarray Studies'. Nucleic Acids Research 43 (7): e47. https://doi.org/10.1093/nar/gkv007.

Roberts, R. Michael, Jonathan A. Green, and Laura C. Schulz. 2016. 'The Evolution of the Placenta'. Reproduction (Cambridge, England) 152 (5): R179-189. https://doi.org/10.1530/REP-16-0325.

Robinson, Mark D., Davis J. McCarthy, and Gordon K. Smyth. 2010. 'edgeR: A Bioconductor Package for Differential Expression Analysis of Digital Gene Expression Data'. Bioinformatics (Oxford, England) 26 (1): 139–40. https://doi.org/10.1093/bioinformatics/btp616.

Rosario, Gracy Xavier, and Colin L Stewart. 2016. 'The Multifaceted Actions of Leukaemia Inhibitory Factor in Mediating Uterine Receptivity and Embryo Implantation'. American Journal of Reproductive Immunology 75 (3): 246–55. https://doi.org/10.1111/aji.12474.

Salleh, Naguib, and Nelli Giribabu. 2014. 'Leukemia Inhibitory Factor: Roles in Embryo Implantation and in Nonhormonal Contraception'. TheScientificWorldJournal 2014: 201514. https://doi.org/10.1155/2014/201514.

Sepp, Mari, Kevin Leiss, Florent Murat, Konstantin Okonechnikov, Piyush Joshi, Evgeny Leushkin, Lisa Spänig, et al. 2024. 'Cellular Development and Evolution of the Mammalian Cerebellum'. Nature 625 (7996): 788–96. https://doi.org/10.1038/s41586-023-06884-x.

Seppälä, Markku, Robert N. Taylor, Hannu Koistinen, Riitta Koistinen, and Edwin Milgrom. 2002. 'Glycodelin: A Major Lipocalin Protein of the Reproductive Axis with Diverse Actions in Cell Recognition and Differentiation'. Endocrine Reviews 23 (4): 401–30. https://doi.org/10.1210/er.2001-0026.

Shukla, Vinay, Jyoti Bala Kaushal, Pushplata Sankhwar, Murli Manohar, and Anila Dwivedi. 2019. 'Inhibition of TPPP3 Attenuates β-Catenin/NF-κB/COX-2 Signaling in Endometrial Stromal Cells and Impairs Decidualization'. The Journal of Endocrinology 240 (3): 417–29. https://doi.org/10.1530/JOE-18-0459.

Silvestri, Audrey, and Hamish M. Fraser. 2007. 'Oestrogen and Progesterone Receptors in the Marmoset Endometrium: Changes during the Ovulatory Cycle, Early Pregnancy and after Inhibition of Vascular Endothelial Growth Factor, GnRH or Ovariectomy'. Reproduction (Cambridge, England) 134 (2): 341–53. https://doi.org/10.1530/REP-06-0266.

Siriwardena, Dylan, and Thorsten E. Boroviak. 2022. 'Evolutionary Divergence of Embryo Implantation in Primates'. Philosophical Transactions of the Royal Society B: Biological Sciences 377 (1865): 20210256. https://doi.org/10.1098/rstb.2021.0256.

Sones, Jennifer L., Audrey A. Merriam, Angelina Seffens, Dex-Ann Brown-Grant, Scott D. Butler, Anna M. Zhao, Xinjing Xu, Carrie J. Shawber, Jennifer K. Grenier, and Nataki C. Douglas. 2018. 'Angiogenic Factor Imbalance Precedes Complement Deposition in Placentae of the BPH/5 Model of Preeclampsia'. FASEB Journal: Official Publication of the Federation of American Societies for Experimental Biology 32 (5): 2574–86. https://doi.org/10.1096/fj.201701008R.

Soneson, Charlotte, Michael I. Love, and Mark D. Robinson. 2015. 'Differential Analyses for RNA-Seq: Transcript-Level Estimates Improve Gene-Level Inferences'. F1000Research 4: 1521. https://doi.org/10.12688/f1000research.7563.2.

Spassky, Nathalie, and Alice Meunier. 2017. 'The Development and Functions of Multiciliated Epithelia'. Nature Reviews. Molecular Cell Biology 18 (7): 423–36. https://doi.org/10.1038/nrm.2017.21.

Stavreus-Evers, Anneli, Erik Mandelin, Riitta Koistinen, Lusine Aghajanova, Outi Hovatta, and Markku Seppälä. 2006. 'Glycodelin Is Present in Pinopodes of Receptive-Phase Human Endometrium and Is Associated with down-Regulation of Progesterone Receptor B'. Fertility and Sterility 85 (6): 1803–11. https://doi.org/10.1016/j.fertnstert.2005.12.018.

Turco, M. Y., L. Gardner, J. Hughes, T. Cindrova-Davies, M. J. Gomez, L. Farrell, M. Hollinshead, et al. 2017. 'Long-Term, Hormone-Responsive Organoid Cultures of Human Endometrium in a Chemically Defined Medium.' Nature Cell Biology 19 (5): 568–77. https://doi.org/10.1038/ncb3516.

Turco, Margherita Y., Lucy Gardner, Jasmine Hughes, Tereza Cindrova-Davies, Maria J. Gomez, Lydia Farrell, Michael Hollinshead, et al. 2017. 'Long-Term, Hormone-Responsive Organoid Cultures of Human Endometrium in a Chemically Defined Medium'. Nature Cell Biology 19 (5): 568–77. https://doi.org/10.1038/ncb3516.

Uchida, Hiroshi, Tetsuo Maruyama, Sayaka Nishikawa-Uchida, Kaoru Miyazaki, Hirotaka Masuda, and Yasunori Yoshimura. 2013. 'Glycodelin in Reproduction'. Reproductive Medicine and Biology 12 (3): 79–84. https://doi.org/10.1007/s12522-013-0144-2.

Uchida, Hiroshi, Tetsuo Maruyama, Masanori Ono, Kuniaki Ohta, Takashi Kajitani, Hirotaka Masuda, Takashi Nagashima, Toru Arase, Hironori Asada, and Yasunori Yoshimura. 2007. 'Histone Deacetylase Inhibitors Stimulate Cell Migration in Human Endometrial Adenocarcinoma Cells through Up-Regulation of Glycodelin'. Endocrinology 148 (2): 896–902. https://doi.org/10.1210/en.2006-0896.

Wetendorf, Margeaux, San-Pin Wu, Xiaoqiu Wang, Chad J. Creighton, Tianyuan Wang, Rainer B. Lanz, Leen Blok, et al. 2017. 'Decreased Epithelial Progesterone Receptor A at the Window of Receptivity Is Required for Preparation of the Endometrium for Embryo Attachment'. Biology of Reproduction 96 (2): 313–26. https://doi.org/10.1095/biolreprod.116.144410.

Winkler, Ivana, Alexander Tolkachov, Fritjof Lammers, Perrine Lacour, Klaudija Daugelaite, Nina Schneider, Marie-Luise Koch, et al. 2024. 'The Cycling and Aging Mouse Female Reproductive Tract at Single-Cell Resolution'. Cell 187 (4): 981-998.e25. https://doi.org/10.1016/j.cell.2024.01.021.

Xie, Yiran, Fangqi Zhao, Nancy Freitag, Sophia Borowski, Yiru Wang, Charlotte Harms, Poh-Choo Pang, et al. 2023. 'Maternal-Derived Galectin-1 Shapes the Placenta Niche through Sda Terminal Glycosylation: Implication for Preeclampsia'. PNAS Nexus 2 (8): pgad247. https://doi.org/10.1093/pnasnexus/pgad247.

Xu, Ling, Yan-Hong Li, Wei-Jie Zhao, Yi-Fei Sang, Jia-Jia Chen, Da-Jin Li, and Mei-Rong Du. 2022. 'RhoB Promotes Endometrial Stromal Cells Decidualization Via Semaphorin3A/PlexinA4 Signaling in Early Pregnancy'. Endocrinology 163 (11): bqac134. https://doi.org/10.1210/endocr/bqac134.

Yan, Wei, and Hugh Clarke. 2017. 'Duplicate: New Chapter for Biology of Reproduction'. Biology of Reproduction, August. https://doi.org/10.1093/biolre/iox090.

Young, Matthew D., and Sam Behjati. 2020. 'SoupX Removes Ambient RNA Contamination from Droplet-Based Single-Cell RNA Sequencing Data'. GigaScience 9 (12): giaa151. https://doi.org/10.1093/gigascience/giaa151.

Yu, Hai-Fan, Zhan-Peng Yue, Kai Wang, Zhan-Qing Yang, Hong-Liang Zhang, Shuang Geng, and Bin Guo. 2017. 'Gja1 Acts Downstream of Acvr1 to Regulate Uterine Decidualization via Hand2 in Mice'. The Journal of Endocrinology 233 (2): 145–57. https://doi.org/10.1530/JOE-16-0583.

Zhang, Yuqing, Giovanni Parmigiani, and W. Evan Johnson. 2020. 'ComBat-Seq: Batch Effect Adjustment for RNA-Seq Count Data'. NAR Genomics and Bioinformatics 2 (3): lqaa078. https://doi.org/10.1093/nargab/lqaa078.

Zheng, Grace X. Y., Jessica M. Terry, Phillip Belgrader, Paul Ryvkin, Zachary W. Bent, Ryan Wilson, Solongo B. Ziraldo, et al. 2017. 'Massively Parallel Digital Transcriptional Profiling of Single Cells'. Nature Communications 8 (January): 14049. https://doi.org/10.1038/ncomms14049.

Licence

Human, macaque and mouse icons were extracted from PhyloPic (http://phylopic.org), and are available for reuse under the Public Domain Mark 1.0 license.

Acknowledgements

We thank C.M. Fovet and F. Relouzat (CEA, Fontenay-aux-Roses, FR) for providing serendipitously collected tissue samples; H. Kaessmann (ZMBH, Heidelberg, DE), C. Dégletagne (CRCL, Lyon, FR) and R. Vento-Tormo (Wellcome Trust Sanger Institute, Hinxton, UK) for sharing protocols and technical advice with tissue collection and single-nucleus sequencing; S. Chouzenoux (Institut Cochin, Paris, FR) for technical advice with cell culture; B. Ouwerling and T. Haaksma (BPRC, Rijswijk, NL) for technical support with tissue collection. We thank the scBiomarkers UTechS platform, C2RT, Institut Pasteur, France, for support in conducting this study. We thank M. Monot and the Biomics platform, C2RT, Institut Pasteur, Paris, France, supported by France Génomique (ANR-10-INBS-09) and IBISA. We thank Muriel Andireu and Vaarany Karunanithy from the Cytometry and Immunobiology Facility CYBIO of the Cochin Institute for their help for single-nuclei processing of macaque sample.

This paper was typeset with the bioRxiv word template by @Chrelli: www.github.com/chrelli/bioRxiv-word-template

Funding

This project was supported by Institut Pasteur (G5 package), Centre National de la Recherche Scientifique (CNRS UMR 3525), Institut National de la Santé et de la Recherche Médicale (INSERM UA12), the European Research Council (ERC) under the European Union's Horizon 2020 research and innovation programme (grant agreement No 851360), and the Inception program (Investissement d'Avenir grant ANR-16-CONV-0005).

Author contributions

A.B. and C.B. designed experiments; A.B., B.R. and A.L. performed experiments with help from M.R. and L.D.; M.A.G., M.D., E.L. and M.S.R. analysed the data; L.F., P.R., P.M.V., L.F., A.C., S.G., L.M. and C.A. performed animal tissue collections; I.K. provided tissue samples and histopathology expertise; M.D., E.L., A.B., M.A.G. and C.B. designed figures; C.B., A.B., M.D. and E.L. wrote the manuscript with input from M.A.G and other authors.

Competing interest statement

The authors declare that they have no competing interests.

Supplementary figures

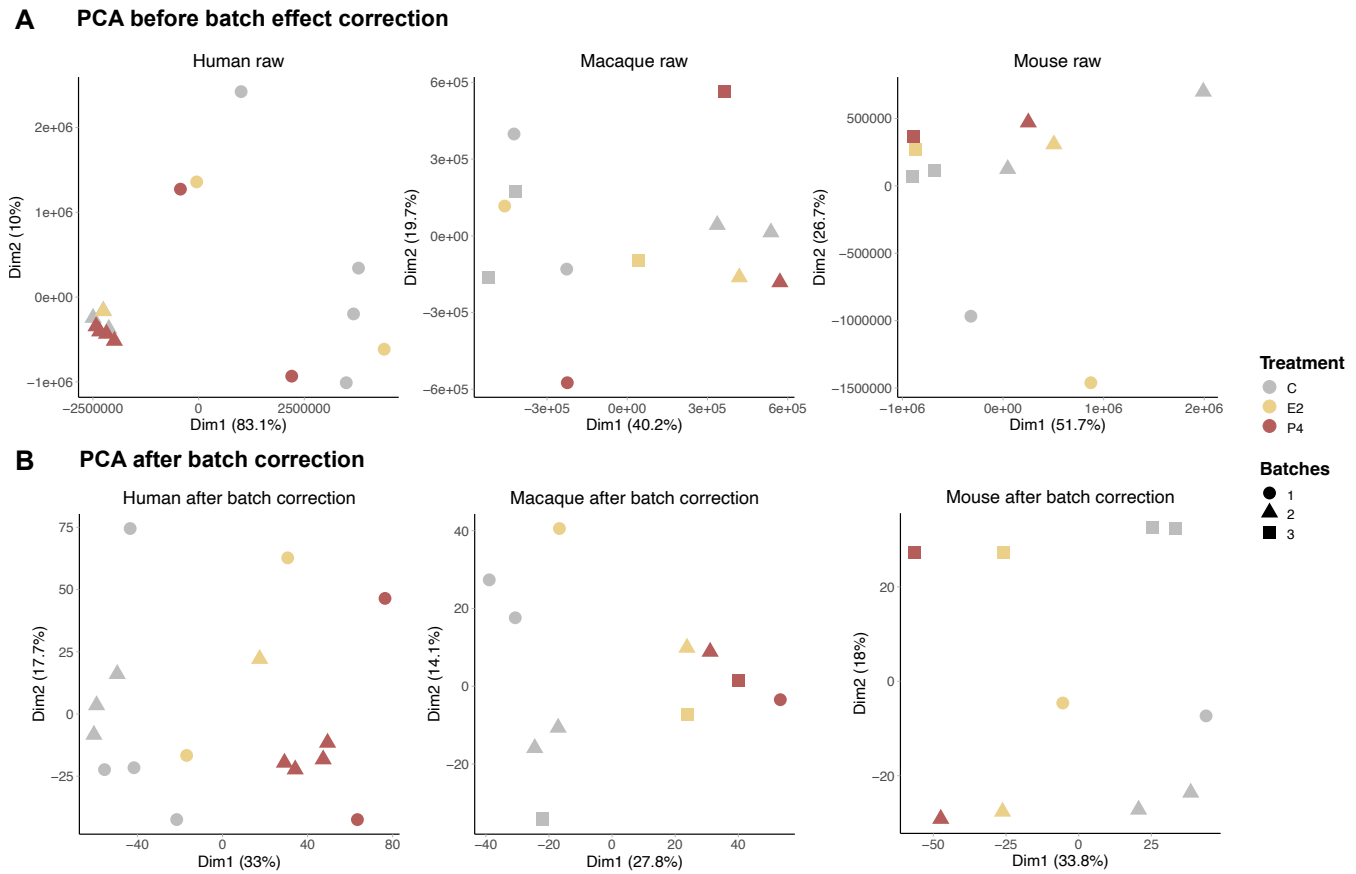

Figure S1: PCA of bulk RNA-seq from human, macaque and mouse organoids. (A) with raw counts **(B)** and counts after batch correction. Samples are coloured by condition. Counts were z-normalised and scaled before PCA.

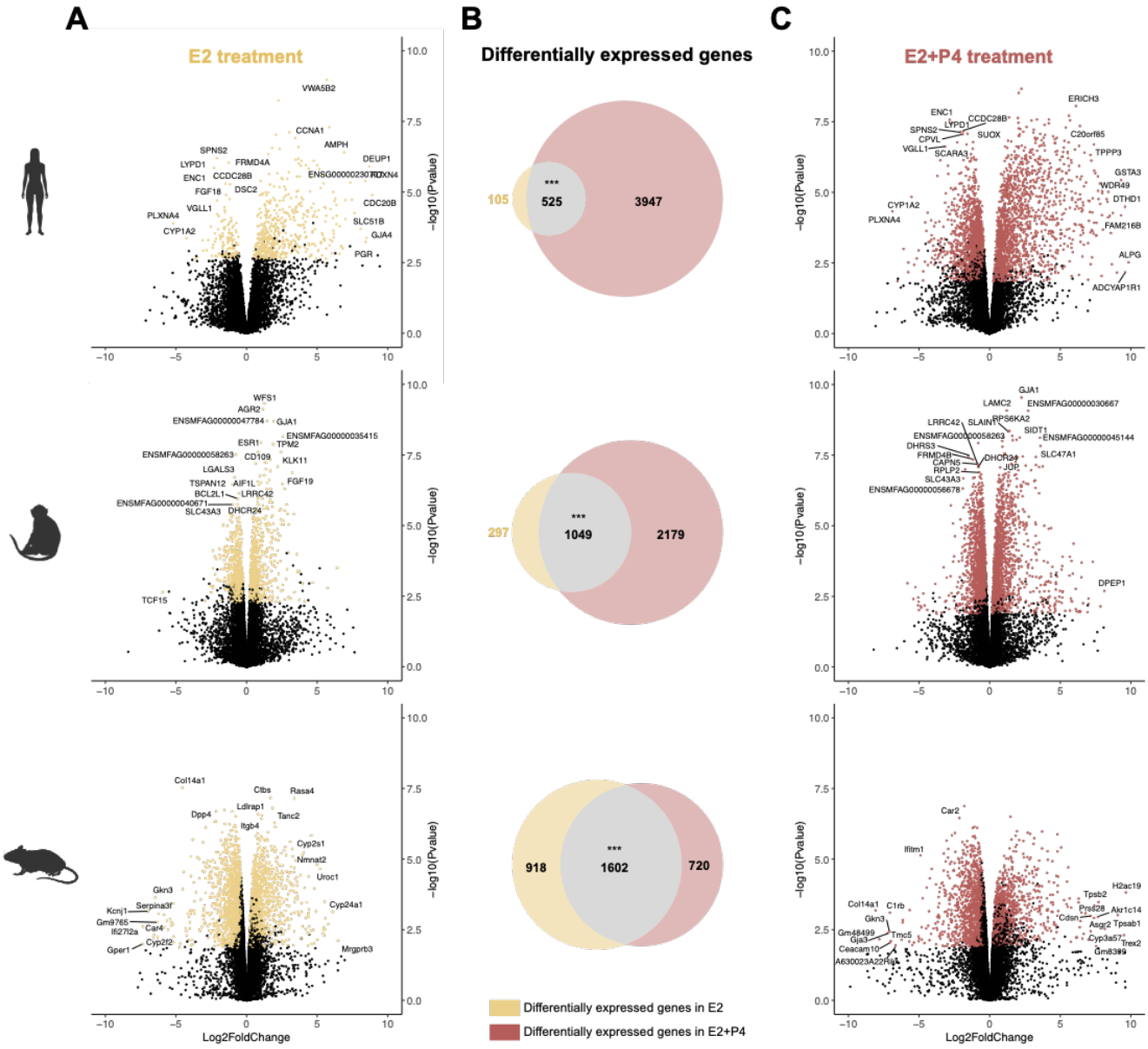

Figure S2: Differential expression analysis in human, macaque and mouse organoids after E2 or E2+P4 treatments. (A,C) Volcano plots of differential gene expression in response to E2 (yellow, **A**) or E2+P4 (red, **C**) treatment for each species. Gene names are reported for the top 10 up- and down-regulated DEG based on highest Euclidean distance to 0. **(B)** Venn diagram of the overlapping DEGs between E2 and E2+P4 conditions, colour intensity represents the representation factor for each species. ***: p-values < 0.001, hypergeometric test, BH adjustment.

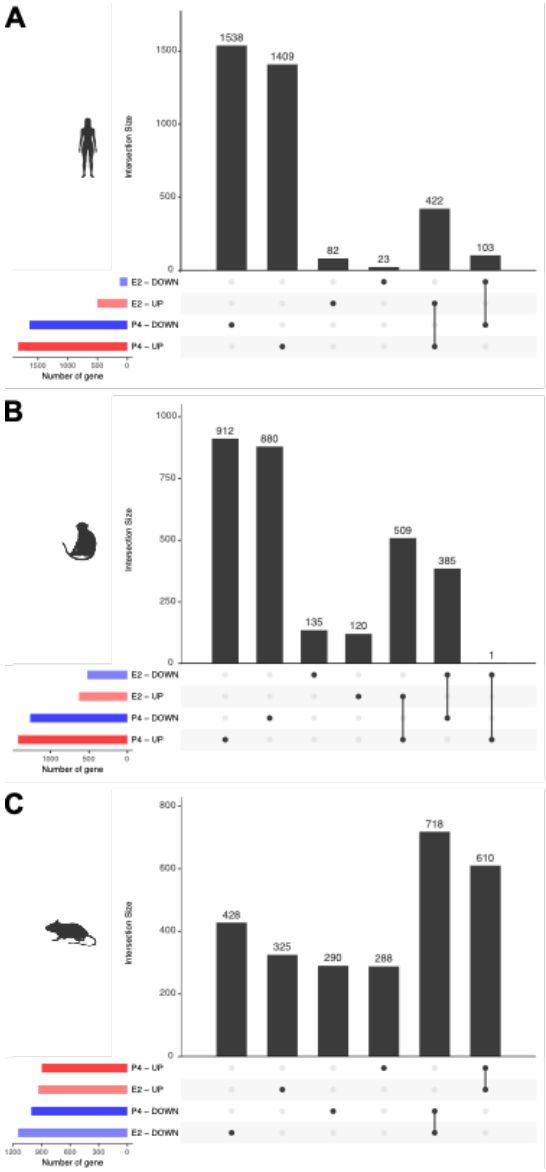

Figure S3: Shared DEG in response to E2 or E2+P4 treatment in each species. Upset plot representing the number of shared genes up- or down-regulated in response to E2 and E2+P4 in **(A)** human, **(B)** macaque and **(C)** mouse.

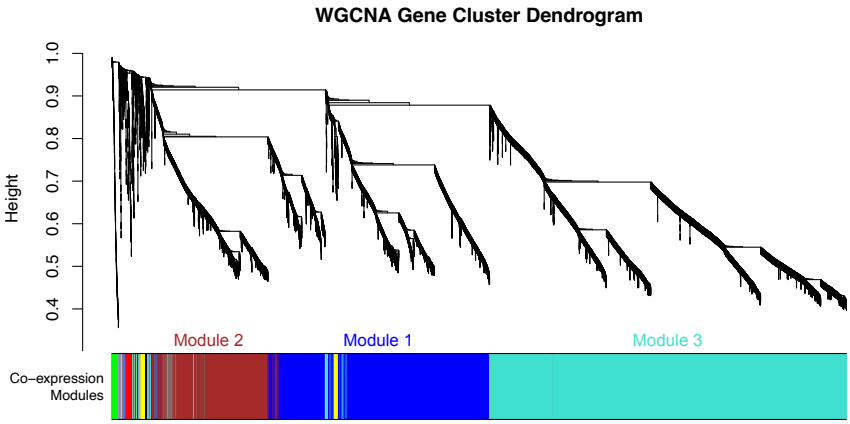

Figure S4: WGCNA dendrogram and gene modules. Clustering dendrogram of gene co-expression measures produced by WGCNA (Weighted Gene Correlation Network Analysis), with dissimilarity based on topological overlap.

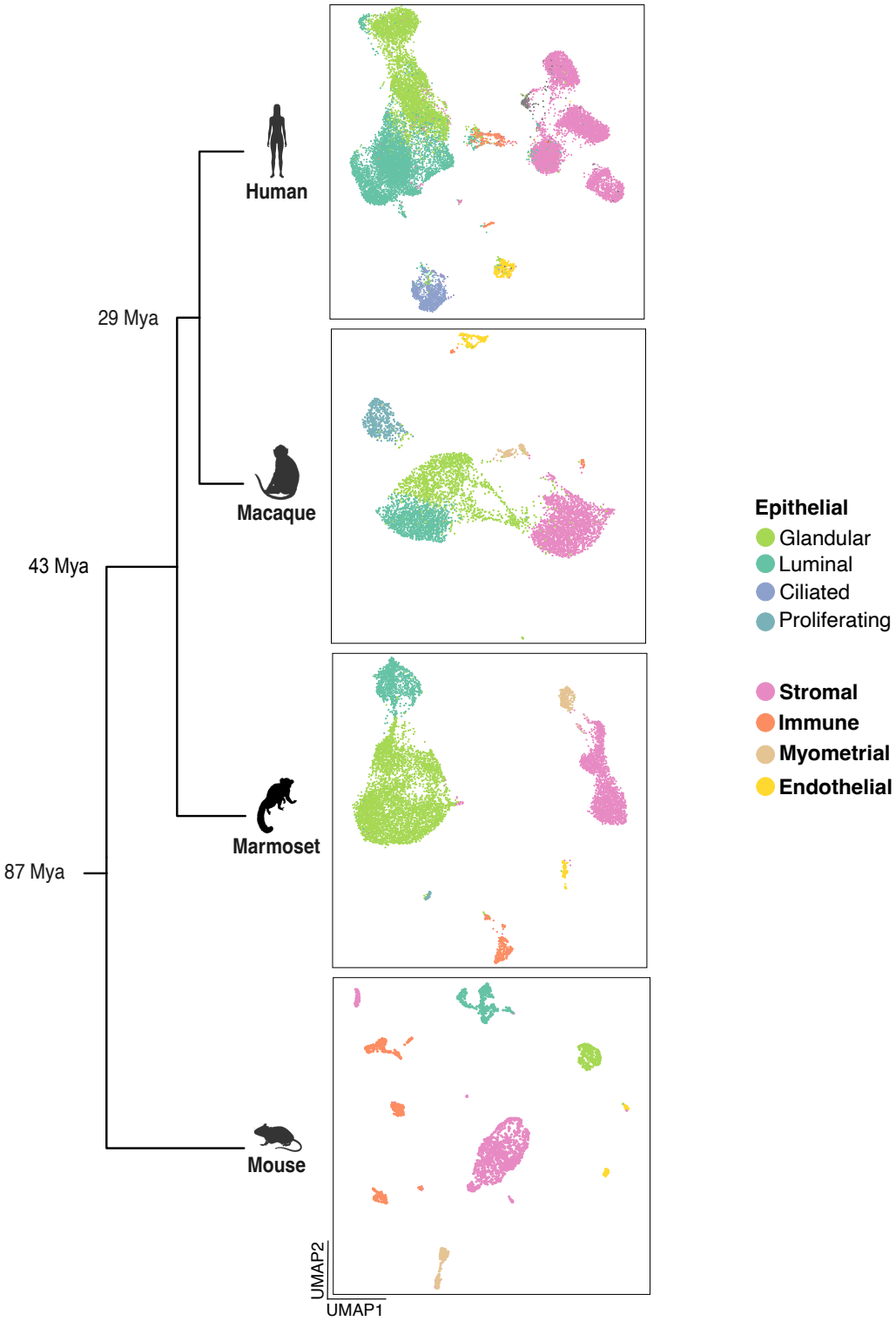

Figure S5: Annotation of endometrial cell types from single-cell RNA-seq data. UMAPs representing the endometrial cell clusters detected in each species (Methods).

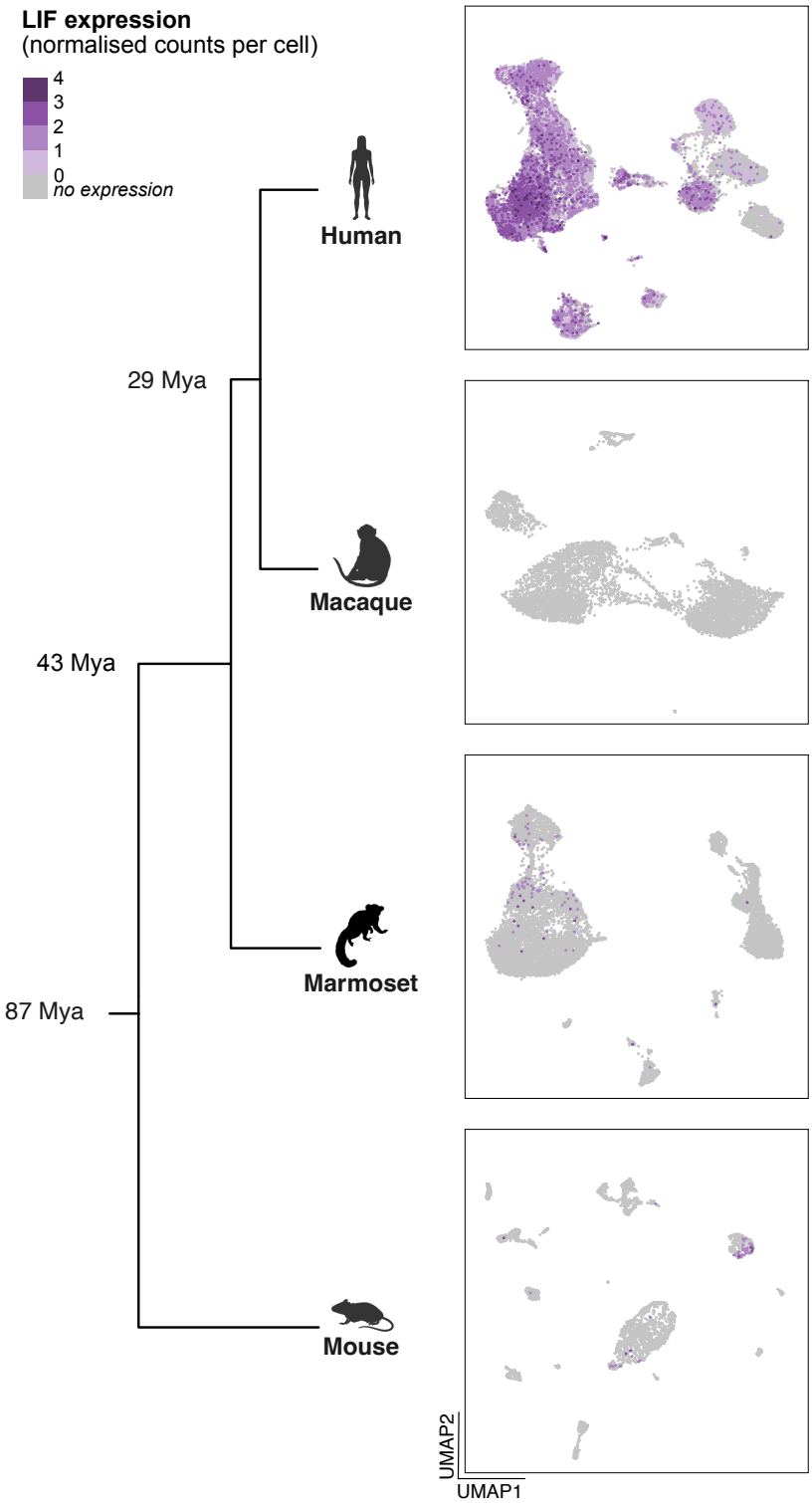

Figure S6: *LIF* expression across all cell types in each species. Gene expression values corresponding to normalised counts by cell (log2 normalised and scaled with scaling factor 10,000) are represented on the UMAP projection of the single-cell data.

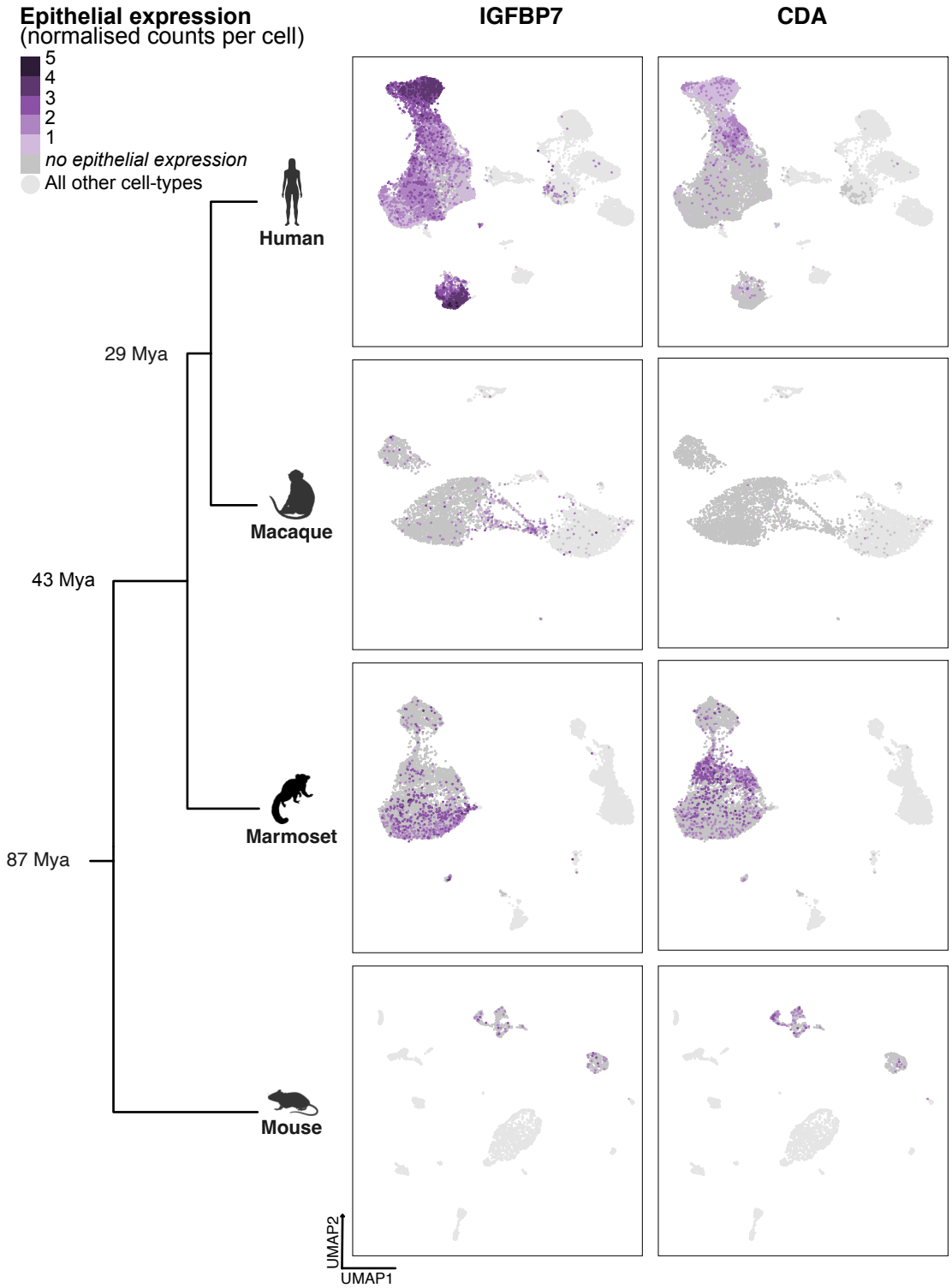

Figure S7: *CDA* and *IGFBP7* expression in epithelial cells. Gene expression values correspond to normalised counts by cell (log2 normalised and scaled with scaling factor 10,000) and are represented for epithelial cells only. Other cell-types are coloured in light grey regardless of *CDA* or *IGFBP7* expression.

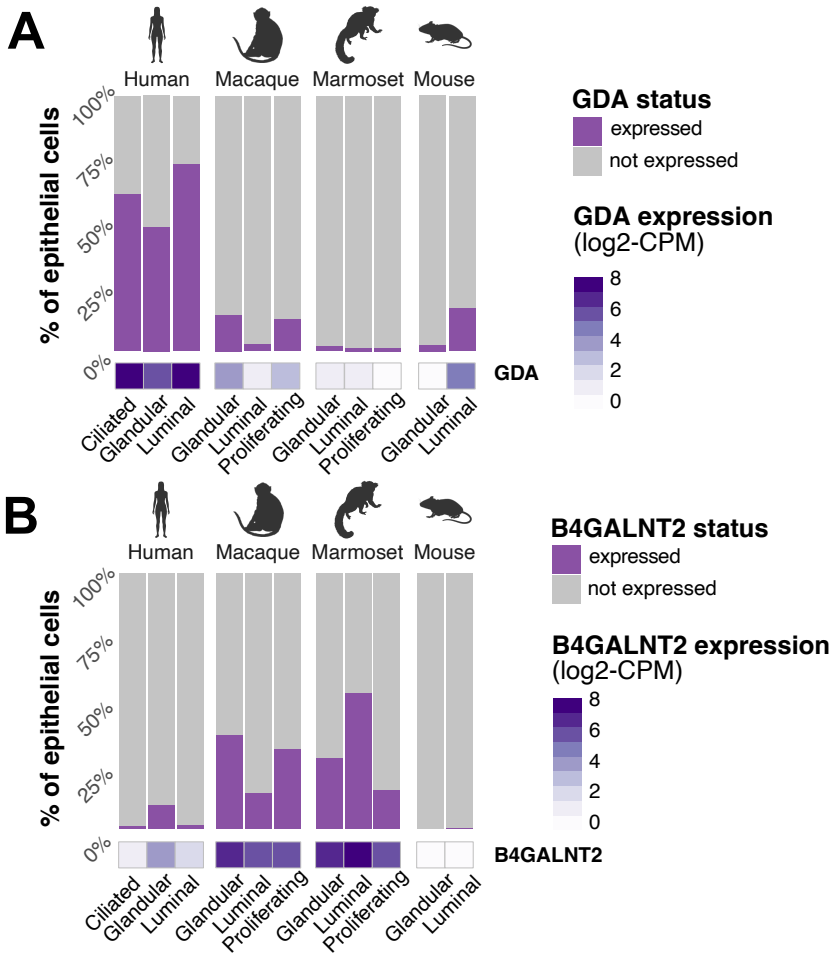

Figure S8: *GDA* and *B4GALNT2* expression in epithelial cell types in each species. Quantitative expression of (A) *GDA* and **(B)** *B4GALNT2* across epithelial subpopulations. Top: proportion of epithelial cells expressing *GDA* or *B4GALNT2* (>0 normalised counts) by epithelial cell type. Bottom: pseudobulk expression of *GDA* or *B4GALNT2* by epithelial cell type. Expression values are represented in log2 CPM.

Supplementary tables

Table S1: DEGs common to all species after each treatment (supplementary Excel file)
Table S2: Shiny GO output for DEGs common to all species after each treatment (supplementary Excel file)
Table S3: Manually curated list of maternal implantation genes (supplementary Excel file)
Table S4: List of genes co-expressed with *LIF* (supplementary Excel file)

Product	Company	Product Number	Final Concentration
Advanced DMEM/F12	Gibco	12634-010	1X
N2 supplement	ThermoFischer	17502048	1%
B27 supplement	ThermoFischer	17504044	2%
Glutamax supplement	ThermoFischer	35050038	2 mM
Penicillin/streptomycin	Gibco	15140-148	1%
Insulin/transferrin/selenium	ThermoFischer	41400045	1%
Nicotinamide	Sigma Aldrich	72340	1 mM
Recombinant mouse EGF	R&D Systems	2028 – EG	50 ng/ml
Recombinant human Noggin	R&D Systems	6057 NG	100 ng/ml
Recombinant human Rspondin-1	R&D Systems	4645-RS	140 ng/ml
Recombinant human FGF-10	Peprotech	100-26	50 ng/ml
Recombinant human FGF2	R&D Systems	233-FB	2 ng/ml
Recombinant mouse WNT3A	Peprotech	31S-20	250 ng/ml
Rock Inhibitor Y-27632*	Merk Millipore	SCM075	10 uM
ALK-4, -5, -7 inhibitor, A8301	Sigma Aldrich	SMLO788	0.5 uM

*Only at seeding and for the first refreshment of the medium at passage 0 (i.e. for 4 days) and at each passage for 48 hours.

Table S5: Growth medium composition for mouse endometrial organoids

Product	Company	Product Number	Final Concentration
Advanced DMEM/F12	Gibco	12634-010	1X
N2 supplement	ThermoFischer	17502048	1%
B27 supplement	ThermoFischer	17504044	2%
Glutamax supplement	ThermoFischer	35050038	2 mM
Penicillin/streptomycin	Gibco	15140-148	1%
Insulin/transferrin/selenium	ThermoFischer	41400045	1%
Nicotinamide	Sigma Aldrich	72340	1 mM
N-Acetyl-L-cycsteine	Sigma Aldrich	A7250	1.25 mM
Recombinant human EGF	R&D Systems	2028 – EG	50 ng/ml
Recombinant human Noggin	R&D Systems	6057 NG	100 ng/ml
Recombinant human Rspondin-1	R&D Systems	4645-RS	70 ng/ml
Recombinant human FGF-10	Peprotech	100-26	50 ng/ml
Recombinant human FGF2	R&D Systems	233-FB	2 ng/ml
Recombinant mouse WNT3A	Peprotech	31S-20	250 ng/ml
Rock Inhibitor Y-27632*	Merk Millipore	SCM075	10 uM
ALK-4, -5, -7 inhibitor, A8301	Sigma Aldrich	SMLO788	0.5 uM
SB202190 (p38i)	Sigma Aldrich	S7067	10 uM

*Only at seeding and for the first refreshment of the medium at passage 0 (i.e. for 4 days) and at each passage for 48 hours.

Table S6: Growth medium composition for macaque endometrial organoids

Antigen	Clone	Species reactivity	Host	Company	Dilution
E-cadherin	4A2	Human, mouse, rat	Mouse monoclonal IgG1	Abcam – ab233766	1/200
Laminin	-	Human, mouse, rat, chinese hamster, mammal, rabbit, sheep, insect	Rabbit polyclonal IgG	Novus Biologicales – NB300-144	1/400
Ki67	-	Human, mouse	Rabbit polyclonal IgG	Abcam – ab15580	1/200
ESR1	E115	Human, mouse, rat	Rabbit monoclonal IgG	Abcam – ab32063	1/200
PGR	SP42	Human, rat, mouse	Rabbit monoclonal IgG	Abcam – ab101688	1/400
PGR	SP2	Human	Rabbit monoclonal IgG	Abcam – ab16661	1/400
acetyl-α tubulin (Lys40)	6-11B-1	Human, mouse, rat	Mouse monoclonal IgG2b	Cell signaling - 12152	1/800

Table S7: Antibodies for immunohistochemical and immunofluorescence staining

Table S8 : Endometrial epithelial organoid bulk RNA-seq quality metrics (supplementary Excel file)
Table S9 : Endometrial snRNA-seq quality metrics (supplementary Excel file)
Table S10 : Marker genes for macaque single-cell clusters (supplementary Excel file)
Table S11 : Marker genes for marmoset single-cell clusters (supplementary Excel file)
Table S12 : Marker genes for mouse single-cell clusters (supplementary Excel file)